NILU : OR 5/99
REFERENCE : O-97074
DATE : MARCH 1999
ISBN : 82-425-1053-9

NILU: OR 5/99

The contribution to nitrogen deposition and ozone formation in South Norway from atmospheric emissions related to the petroleum activity in the North Sea

S. Solberg, S.-E. Walker, S. Knudsen, M. Lazaridis, H. J. Beine and A. Semb

Contents

Page

Summary

On behalf of the Norwegian Oil Producers' Association (OLF), the Norwegian Institute for Air Research (NILU) has been contracted to evaluate the effects of the atmospheric emissions from the oil and gas exploration activity in the Norwegian sector of the North Sea. Deposition of nitrogen and formation of boundary level ozone in Southern Norway due to North Sea emissions of nitrogen oxides (NO_x), carbon monoxide (CO) and volatile organic compounds (VOC) have been studied. The atmospheric processes have been simulated with numerical models developed during the project. The study reported here is a follow-up project after a first phase previously reported by Semb et al. (1996).

Both the emission data themselves and the handling of the emissions in the model simulations have been modified since the report by Semb et al. (1996). New updates for the VOC emissions from loading buoys have been included, increasing the VOC emission estimate for loading buoys from 82 ktonnes/year to 137 ktonnes/year. The VOC emissions from the Norwegian petroleum sector in the North Sea were estimated at about 179 ktonnes (VOC)/year, which is more than half of Norway's total VOC emissions when compared with previous national estimates. The national total should, however, be modified according to the updated emission estimates for the loading buoys to be comparable. The data indicate a NO_x emission in 1992 from the Norwegian petroleum sector in the North Sea of about 45 ktonnes (NO_2)/year, which corresponds to approximately 70% of the total road traffic emissions in Norway.

The most important change in the handling of the emissions in the model was to distribute the emission sources into a number of lumped megasources and the rest to gridded area sources. The main individual emission sources were combined into 20 megasources containing the major fraction of the emissions. The megasources were then modelled by the photochemical plume model Fotoplume developed during this project. The rest of the emissions (i.e. the minor sources) were modelled as area sources using the EMEP oxidant model, which is a European scale trajectory model. The interface between Fotoplume and the EMEP oxidant model was significantly improved as part of this work. An elaborate model procedure for estimating the contributions from the North Sea emissions, separate from all other influence, was designed in order to avoid "noise" introduced by incompatibilities between the numerical models.

The calculated contributions show maxima of 40-50 mg (N)/m^2 from the Norwegian sector and 20-30 mg (N)/m^2 from the British sector to the nitrogen deposition in the coastal areas of Hordaland and Sogn og Fjordane in 1992. This makes a total contribution of 60-80 mg (N)/m^2 in this area for Norwegian and British sector taken together. The largest *relative* contribution from the North Sea is found further north, in Møre og Romsdal, with maximum values of 10-13% for each of Norwegian and British sector compared to the total nitrogen deposition in 1992 including both oxidised and reduced nitrogen. Taken together the petroleum activity in the North Sea thus is calculated to contribute approximately 20% in this region. Note, however, that the emissions from the North Sea only contribute

to the oxided nitrogen deposition whereas the measured deposition also includes *reduced* nitrogen (ammonia). The calculations give a marked maximum zone in N-deposition from the North Sea emissions along the coast, whereas the calculated deposition drops inland. The calculations indicate only a minor contribution from the North Sea emissions to N-deposition in the most exposed areas in the southern part (Agder).

To evaluate the effect of changing meteorology from one year to another, the calculations were performed also with meteorology for 1995 but with the same emissions as for 1992. The calculated contributions from the North Sea to the nitrogen deposition, using 1995-meteorology gives lower deposition values as compared to 1992. This regards particularly the contribution from Norwegian sector. The maximum total N-deposition is calculated to be 20-25 mg (N)/m^2 for emissions from each of Norwegian and British sector in 1995, totalling 40-50 mg (N)/m^2 from the petroleum sector of the North Sea. With 1995-meteorology the maximum area of influence from the Norwegian sector is displaced somewhat to the south. The geographical pattern of N-deposition of North Sea emissions in 1995 is, however, rather similar the one calculated for 1992. The calculations give a maximum deposition zone along the coast in 1995 as in 1992. As the same emission data (for 1992) were used in both the calculations for 1992 and 1995, the differences in the calculated North Sea contribution is purely due to meteorological differences.

The model was also used to estimate the contributions to harmful ozone exposure levels, using the so-called AOT40 index. AOT40 is defined as the integrated ozone exposure above 40 ppb during the growth season, and is normally expressed in the unit ppbhours. In 1992 the observed AOT40 for coniferous/ meadows was high in South Norway peaking at 13,000 ppbhours in Agder, and in the range 6000 – 9000 ppbhours else. The AOT40 values in 1995 were lower, peaking at 5000 – 6000 ppbhours in Agder.

In 1992 the Norwegian sector of the North Sea is calculated to contribute up to 325 ppbhours near Stad. The calculations indicate contributions from Norwegian sector of 130-200 ppbhours in a zone along the coast from Rogaland to Trøndelag, and less than 100 ppbhours else. The contribution from British sector in 1992 is less, peaking at 169 ppbhours in Rogaland, and else mostly values less than 100 ppbhours. The results indicate that emissions from British and Norwegian sector separately contribute to less than 5% each of the AOT40 values for coniferous/meadow.

The calculated influence to the AOT40 value in 1995 is lower (in absolute units) than in 1992. Emissions from Norwegian sector are calculated to contribute with 120-130 ppbhours at most in some coastal areas of Hordaland and Sogn og Fjordane. In other areas the contribution from Norwegian sector is calculated to be less than 100 ppbhours. The contribution from British sector is also less in 1995 compared with 1992, and is lower than 100 ppbhours in all receptor points. Relative to the observed AOT40 the calculated percentage contributions from the North Sea were similar using 1992 meteorology and 1995 meteorology. This is because both the observations and the calculated North Sea contributions were lower in 1995 compared to 1992.

The model calculations in this report are compared with the values given in the previous report by Semb et al. (1996). It is clear that the new version of Fotoplume in general calculates much lower contributions to the N-deposition than previously. To check the reliability of the model, the model was used to calculate the overall fraction of nitrogen emitted in the North Sea which is deposited in the receptor points in Southern Norway. The calculations indicate that 13% of the nitrogen emitted from Norwegian sector is deposited in the receptor points for 1992 as a total. This is slightly less than one would expect based on a very simple consideration of wind transport and deposition efficiency. The results in the previous report by Semb et al. (1996) indicated much higher deposition from the North Sea emission sources. This shows that the model development applied since the previous reporting, and in particular the parameterisation of deposition processes, have given more realistic model results.

For the ozone calculations, it is not straightforward to compare the new calculations with the previous results. However, it is quite clear that the new calculations also give substantially lower contributions from the North Sea emissions to the AOT40 values than calculated previously. This is due to a generally improved model with regard to deposition processes, dynamical processes (atmospheric mixing) as well as an improved interface to the regional EMEP oxidant model. It is, however, also to a large extent due to a more sophisticated procedure for estimating the AOT40 index.

The contribution to nitrogen deposition and ozone formation in South Norway from atmospheric emissions related to the petroleum activity in the North Sea

1. Introduction

The offshore petroleum activity in the North Sea contributes significantly to the total national atmospheric emissions of NO_x (NO_x = NO+NO_2), CO (carbon monoxide) and VOC (volatile organic compounds) in Norway. In 1995 the total NO_x emissions from petroleum related activity in the Norwegian sector of the North Sea was only slightly less than the total NO_x emissions from all road traffic in Norway and constituted 25% of Norway's NO_x emissions. The share of VOC emissions was higher, in 1995 about 50% of Norway's total VOC emissions stemmed from petroleum activity in the North Sea.

In addition, the gases are emitted upwind of Norway's main land, and are thus frequently transported towards the coast. The travel time from the emission area to the Norwegian coast is of the same order as that needed for the formation of ozone and nitrates in the atmosphere. Furthermore, transport across the sea implies negligible deposition of NO_x and ozone (which both would be deposited over land). NO_x converted to HNO_3 is absorbed by the water surface, however.

Taken together this situation makes it important to evaluate the effects of the North Sea emissions for acid deposition and ozone exposure in South Norway. Limited studies have previously been performed for e.g. emissions from the Troll platform (Simpson, 1992) and from the loading at Sture (Semb and Solberg, 1993). On behalf of the Norwegian Oil Industry Association (OLF) the Norwegian Institute for Air Research (NILU) has developed the numerical model Fotoplume, specially designed to improve the simulation of emissions and atmospheric transport and chemical transformations of pollutants from offshore oil and gas production in the North Sea. NILU also prepared a report containing a theoretical outline of the chemical transformation and deposition of the North Sea emissions (Semb et al., 1995).

The calculations with the Fotoplume model were first reported by Semb et al. (1996), and the results were subject to an external review by Prof. Trond Iversen at the University of Oslo. Based on his recommendations and the experience and views within the steering group at OLF and the researchers at NILU, it was decided to further refine and develop certain aspects of the Fotoplume model and then to rerun the previous calculations with an improved model.

As part of this second phase of the project for OLF, Solberg et al. (1998) prepared a report presenting an evaluation and validation of the model based on comparison with observations, and also containing proposals for model developments.

The present report is the final report in this second phase, giving firstly an outline of the model development, and, secondly, the calculated nitrogen deposition and ozone exposure with the updated model.

During the same time period, the Fotoplume model has been applied in several environmental impact assessment studies, e.g. for petroleum related emissions at Haltenbanken (Knudsen et al., 1996a), for a planned gas power plant at Kollsnes (Knudsen et al., 1996b) and for future emissions at the Norwegian sector of the North Sea (Solberg et al., 1999).

2. Background

A comprehensive outline of the physical and chemical processes leading to acid deposition and ozone formation is not included in the present report. For this, the reader is referred to the background report by Semb et al. (1995). A short description of the most basic processes is given below.

In the sunlit atmosphere, hydrocarbons and nitrogen oxides enter into numerous photochemical reactions which gradually convert the hydrocarbons to oxygenated compounds and eventually to carbon dioxide. The nitrogen oxides are not consumed in this process, but are only cycled between nitrogen monoxide (NO) and nitrogen dioxide (NO_2). Each cycle generates one ozone molecule. Thus, the amount of produced ozone depends on how many cycles the nitrogen oxides go through before they are ultimately lost through other processes. Usually the ozone production potential for each NO_x molecule is between 2 and 6. The dominant loss process for NO_x ($NO+NO_2$) is by reaction with free radicals which converts NO_x to gaseous nitric acid. Gaseous nitric acid may subsequently dissolve in water droplets or be converted to nitrate particles. Both nitric acid and nitrate particles may then be lost by precipitation and thus be deposited as nitrate to the ground, the so-called wet deposition. Nitric acid is very water-soluble and is therefore readily absorbed by the sea surface and by precipitation. The deposition velocity over the sea varies with the wind velocity, but is typically of the order of 0.5 cm/s, corresponding to a loss in the airborne concentrations of about 2%/h.

During night-time, nitrogen dioxide is converted to nitric acid and to nitrate in particles by reaction with ozone. This reaction is slower than the reaction with hydroxyl radicals in sunlight. During summer, however, high concentrations of ozone and long periods of sunlight cause nitrogen oxides emitted from oil extraction activities to be converted to nitric acid and nitrates before the air reaches the Norwegian coast. These emissions therefore contribute little to the concentration level of nitrogen oxides at the Norwegian mainland.

The deposition of nitrogen oxide and nitrogen dioxide to the sea surface is negligible. Dry deposition to the ground is, however, effective for nitrogen dioxide as well as nitric acid and nitrate particles. Deposition rates of nitric acid and particulate nitrate are increased over land, mainly because of the increased surface aerodynamic roughness.

3. Emissions

Figure 1 shows the influence area used in the calculations. The grid is the EMEP 50 km × 50 km grid system and the black dots, placed in the middle of the grid squares at the Norwegian coast, are the receptor points used. The small square symbols mark the monitoring sites used for comparison with the model calculations, and are, following the coast from North to South, Kårvatn, Voss, Skreådalen, Birkenes and Langesund.

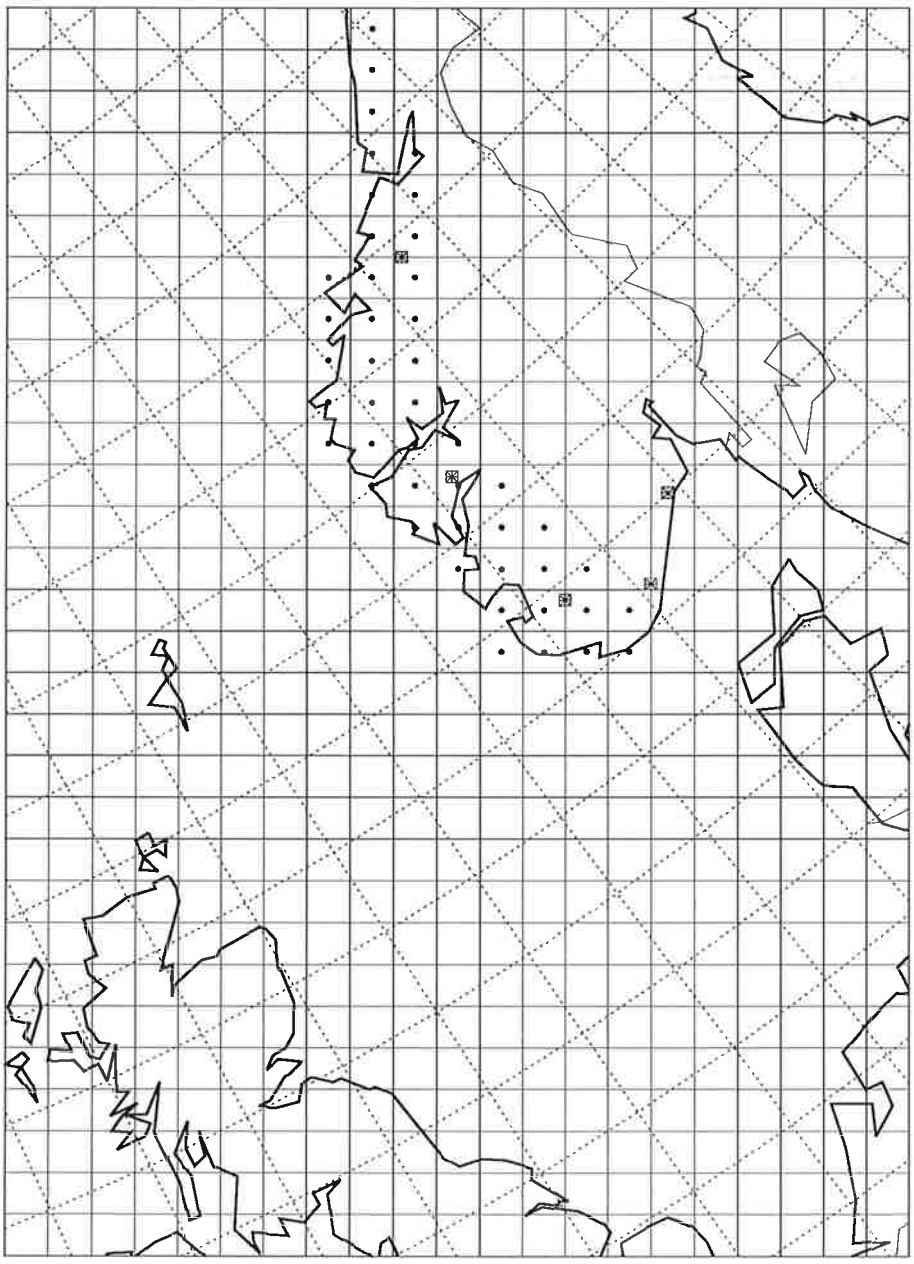

Figure 1: Map showing the model domain used in the calculations and the corresponding 50 km× 50 km grid squares. The dots mark the receptor points, and the square symbols mark the Norwegian background monitoring sites Kårvatn, Voss, Skreådalen, Birkenes and Langesund listed from north to southeast.

A complete listing of the emission data used in this work is given in Appendix A. A summary of the emission data is given in Table 1. These data show that the emissions from the petroleum sector in the North Sea represent a considerable contribution to the national total emissions for Norway. The NO_x-emission from the Norwegian petroleum sector in 1992 was almost 70% of the NO_x-emissions from road traffic in Norway (in 1995). A large part of Norway's VOC-emissions stems from petroleum related emissions in the North Sea. Table 1 indicates that more than half the national VOC emissions are from the petroleum sector in the North Sea. As the numbers in Table 1 are taken from separate sources of information, they may not be directly comparable. The indicated total Norwegian VOC is too low according to the updated VOC emission data for loading buoys given in the table below.

Table 1: Emissions of NO_x and VOC in 1992 from Norway as a whole, from Norwegian road traffic in 1995 and from the Norwegian and British petroleum sector in the North Sea in 1992.

	NO_X-emissions (1000 tonnes (NO_2)/year)	VOC-emissions (1000 tonnes VOC/year)
National total for Norway 1992[a)]	216	323
Total road traffic, Norway, 1995 [b)]	67	64
Norwegian petroleum sector, North Sea, 1992	45	179
British petroleum sector, North Sea, 1992	89	16

[a)] EMEP MSC-W (1998)
[b)] Data for 1995 from Central bureau of Statistics Norway

The emission data in this work were based on the same data as previously, including emissions of NO_x, CO and VOC specified for a total of 488 single sources for the British and the Norwegian sector of the North Sea for 1992. Several modifications and corrections have been carried out on the model, however.

3.1 Updated emission estimates of VOC from loading buoys

Since the previous study was performed, it had been discovered that the VOC emissions from loading buoys were substantially underestimated in the previous data. The VOC emissions from loading therefore had to be changed according to new estimates. Table 2 shows the old and the new, updated VOC emissions from the loading buoys.

Table 2: VOC emissions (tonnes VOC/year) used previously as well as the new estimates applied in the present calculations.

Platform installation	Loading buoy	Old VOC emission estimate (t/y)	New VOC emission estimate (t/y)
Statfjord	OLS-A	23293	34067
Statfjord	OLS-B	23293	34067
Statfjord	SPM-C	23293	34067
Gullfaks	SPM-1	6310	17275
Gullfaks	SPM-2	6310	17275
SUM		**82499**	**136751**

3.2 Corrected VOC speciation for different source categories

The VOC speciation, i.e. the relative distribution profile used to define the emission rate of the models individual VOC species (ethane, ethene etc.) was modified compared to the previously used profiles. The reason for this was that the VOC profile previously used was not considered to be appropriate for some of the emission source categories. This regarded in particular the loading buoys, where 10%, 5%, and 15% previously were distributed as ethene, propene and xylenes, respectively. Table 3 gives the VOC distribution for different source categories used in the present calculations.

Table 3: Updated VOC distribution functions used in the present calculations. All numbers refer to weight percent.

	Loading buoys	Flare	Turbines	Transport*
C_2H_6	34	12.50	18.75	5.7
C_4H_{10}	66	12.50	25.00	18.0
C_2H_4		6.25	12.50	12.0
C_3H_6		18.75	12.50	4.6
C_8H_{10}		37.50	25.00	10.6
HCHO		7.50	3.75	5.9
CH_3CHO		5.00	2.50	4.0
CH_3OH				
C_2H_5OH				39.2
SUM	100	100	100	100

* Includes diesel engines, helicopter traffic, supply ships and stand by ships.

The distribution functions in Table 3 were constructed from different sources of information. The loading buoys give only alkanes, and the weight distribution shown in Table 3 was based on emission measurements at Sture in 1993 performed by Det Norske Veritas, DNV (Olsen et al., 1993). The model chemistry necessarily has to be simplified and thus all alkanes are represented by the two compounds ethane and n-butane. Emissions of ethane and propane, reported by DNV, were allocated to the model as ethane, whereas all other alkanes were allocated to the model as n-butane.

The VOC emission distribution for flaring and turbines was kept constant, except that a share of 20%, previously allocated to methane, now was distributed onto the VOCs shown in Table 3. The reported total VOC emissions do not include methane.

The VOC emission distribution for transport, given in Table 3, was adopted from the profile used in the standard trajectory EMEP model for UN-ECE category 8, "Other Mobile Transport" ("other" as compared to category 7 – road traffic) which includes emissions from ships.

In addition to the source categories given in Table 3, the three categories "cold vent", "fugitive", and "other sources" were given in the original emission data.

These source categories were given the same VOC distribution as loading buoys (for "cold vent" and "fugitive") and traffic (for "other sources").

3.3 Lumping of emission point sources

Compared to the emission data used previously, the lumping of individual point sources were changed. In the previous calculations, all individual sources were grouped into so-called megasources according to installation numbers. The idea was to represent each installation by one megasource in the Fotoplume calculations. A lumping of the individual sources was obviously needed. Originally the emission data consisted of a total of 488 sources when both the Norwegian and British sector were included, as shown in Figure 2. Many of these sources were close to each other and impossible to resolve as individual stacks in the model. This previously applied lumping reduced the number to approximately 120 megasources.

In the present calculations, an alternative approach was applied where the original individual sources were grouped according to their location and internal distance. Based on the original emission data, a set of megasources was constructed with the constraint that no individual source should be more than 6 km away from any of the other stacks allocated to that megasource. 6 km may seem as a rather large scale compared to the very detailed and fine-structured original emission data.

However, this scale is representative of the plume dimensions after a few hours, and was chosen as the best value both with regard to the mixing of plumes and to retain the fine resolution compared to the underlying 50 km resolution in the emission grid cells for the trajectory model.

Furthermore, compared to the previously reported calculations (Semb et al., 1996) the procedures for the model calculations were changed. Based on the experience with the different model advantages and disadvantages, the emissions were split into two parts. A sorting according to NO_x emission rates showed that nearly 80% of the emission from Norwegian sector in the North Sea stemmed from the 20 largest megasources (lumped on a 6 km resolution). Thus, the number of large point sources (LPS) modelled by Fotoplume was reduced to these 20 point sources. Due to the lumping of the original single stacks, these 20 megasources also contained the dominant VOC sources, which means that the loading buoys were included. The remaining emissions from Norwegian sector as well as all the British emissions were distributed to their corresponding 50 km $\times$ 50 km grid square, and their contribution was calculated by the EMEP oxidant model.

Table 4 shows the emission numbers for NO_x, CO and VOC from the 20 megasources in the Norwegian sector. As indicated by Table 4, the megasources contribute 78% of the total NO_x emission from Norwegian sector and 98% of the VOC emission. Figure 3 shows the location of the 20 Norwegian megasources.

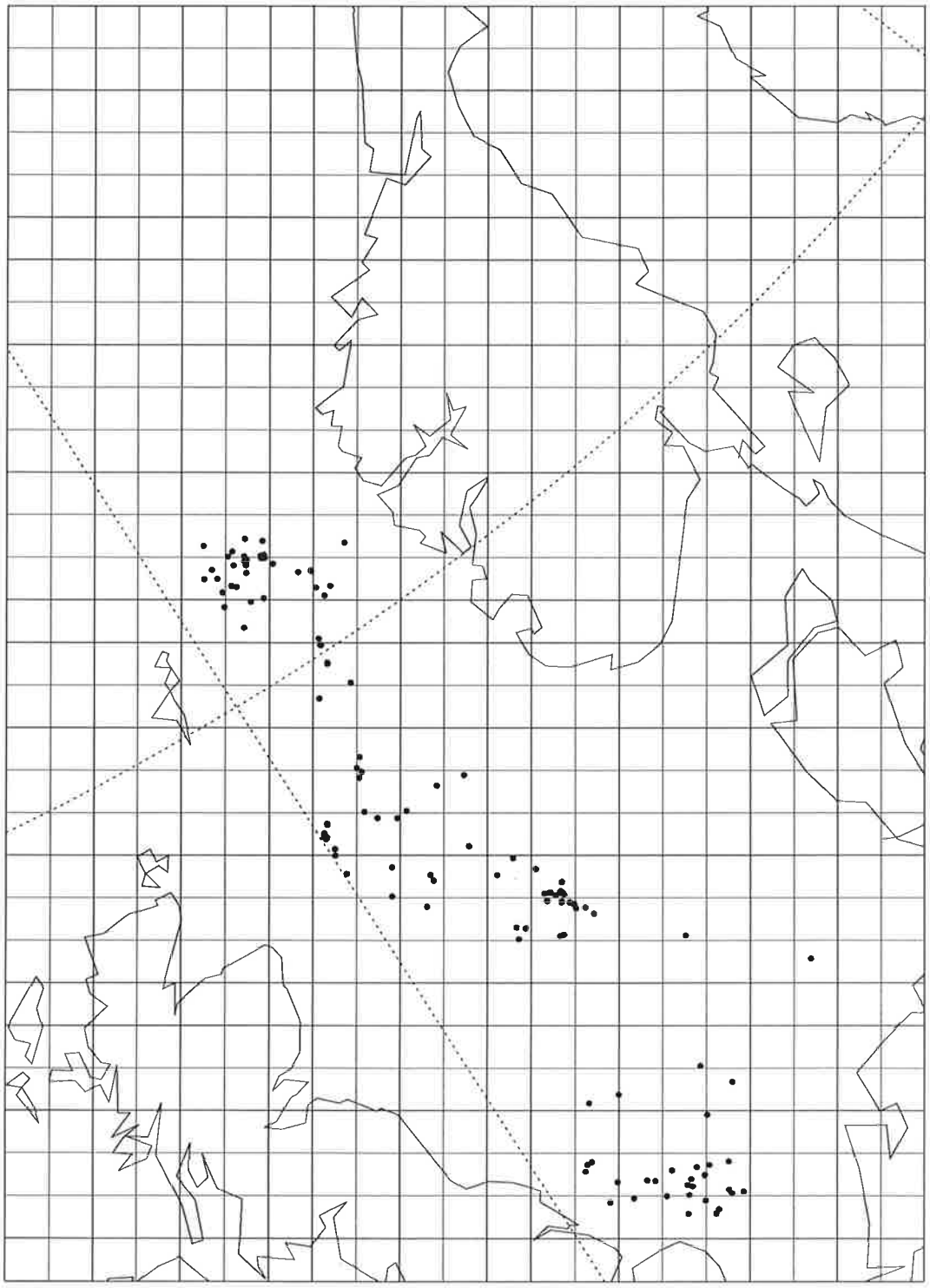

Figure 2: Location of the 488 individual emission sources in the North Sea (British and Norwegian sector).

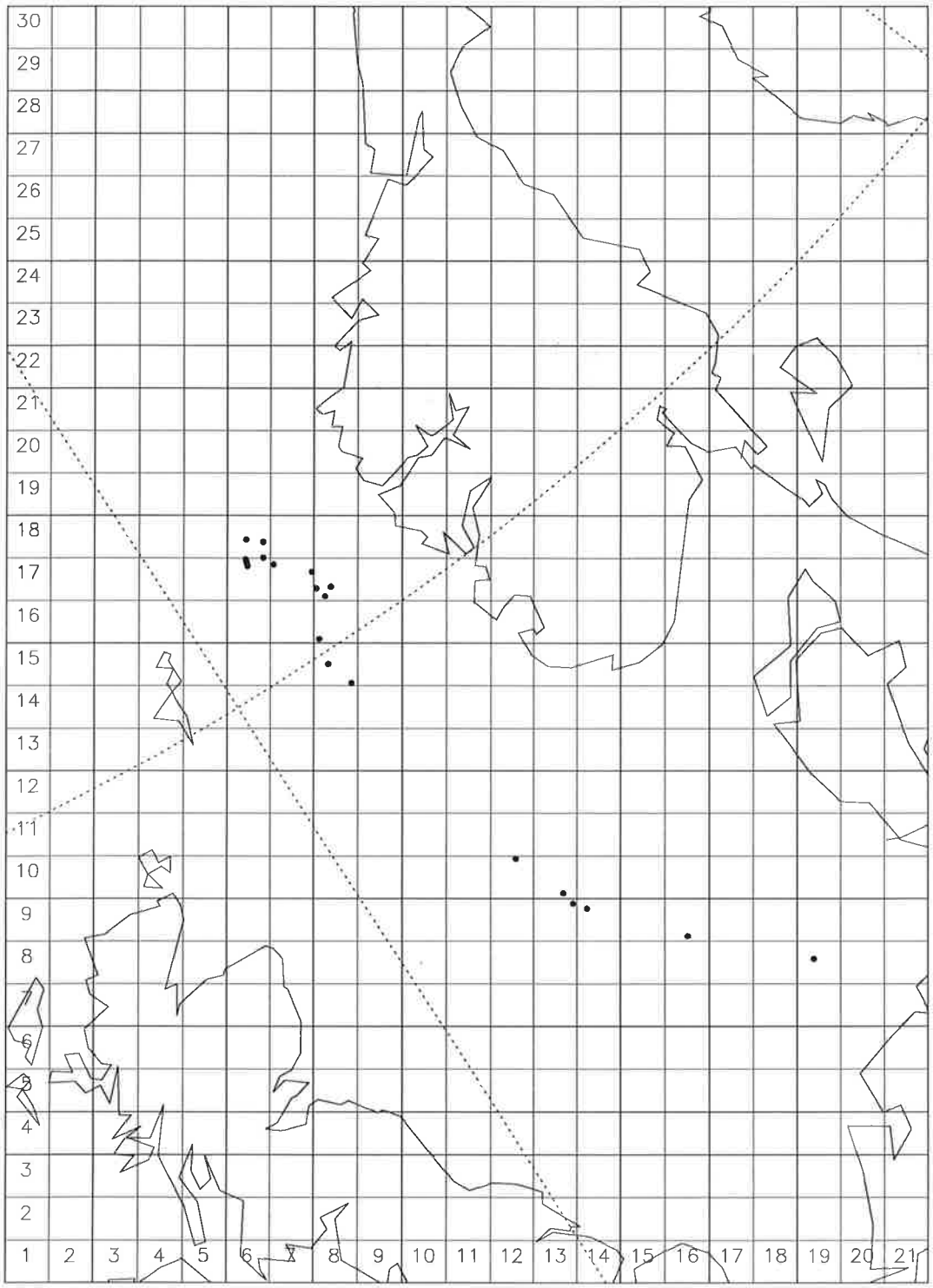

Figure 3: Location of the 20 Norwegian megasources used in the Fotoplume calculations.

The procedure of splitting the emissions is justified by the fact that the advantage by an LPS model, as Fotoplume, is the capability to simulate the transport, diffusion, and photochemical reactions taking place within single emission plumes. A region with several low and moderate, nearby sources is, on the other hand, in practice not possible to simulate with a photochemical puff-trajectory model, and in reality requires some sort of adaptive grid model (Eulerian or Lagrangian). Besides, the basis for developing the Fotoplume model in the first place was to take account for non-linear differences in the model calculations between an Eulerian (grid point) model which smooths all emissions to a certain resolution and a puff trajectory model. The non-linear effects from not including all the smaller point sources in the Fotoplume model will probably be of minor importance.

3.4 Emissions from shuttle tankers during transport

In the previous calculations all emissions from shuttle tankers during transport between the place of loading and unloading were allocated to the place of loading. These emissions contributes significantly to the NO_x emissions and the former procedure is a simplification which lead to too high emissions allocated to the loading platforms.

In the present study the emissions from shuttle ships during transport were distributed to the 50 km $\times$ 50 km grid squares along assumed ship tracks. Data regarding frequency of the different ship routes were used to construct simplified area emission fields. The total emission was evenly distributed in space and time along each track. Annual average emission rates in the grid squares crossed by the ship tracks were then calculated and used in the EMEP oxidant model calculations.

Compared to the previous method where all shuttle ship emissions were allocated to the loading platform, the new procedure will reduce the effect of these emissions. The reason for this is obvious – when the emissions are spread over a large area the contribution to acid deposition and ozone formation is also spread over a large area compared to allocating all emissions to single stack close to the receptor region.

The emission rates from the shuttle tankers during transport and from all remaining sources (allocated to the grid squares) in the Norwegian sector is also shown in Table 4.

Table 4: The emissions from Norwegian sector applied in the model calculations, showing the annual emissions from each of the 20 megasources (explained in the text), the shuttle ships (during transport), and the total from all other sources. The x and y indexes refer to the grid numbering given in Figure 3.

Emission source type	No.	x	y	NO_x emissions (tonnes (NO_2)/year)	CO emissions (tonnes CO/year)	VOC emissions (tonnes VOC/year)
Megasources	1	13	10	7895	2373	1438
	2	6	17	4274	1121	68485
	3	6	18	4049	1047	34872
	4	8	17	2478	573	198
	5	6	17	2082	538	68353
	6	6	17	1878	494	123
	7	7	17	1370	378	139
	8	14	9	1255	303	210
	9	6	18	1226	293	138
	10	16	9	1173	317	249
	11	19	8	1155	312	254
	12	8	17	1100	294	121
	13	8	17	897	288	62
	14	8	15	811	258	453
	15	13	9	734	200	342
	16	12	10	687	178	102
	17	7	17	619	186	44
	18	8	15	472	123	157
	19	6	18	463	139	33
	20	8	16	459	138	33
	Sum			**35076**	**9550**	**175809**
Shuttle ships	**Sum**			**6658**	**2234**	**1332**
Other sources	**Sum**			**2998**	**904**	**1454**
Total sum				**44732**	**12688**	**178595**

3.5 Emissions from British sector

The aim of the project was to estimate the contribution to nitrogen deposition and ozone exposure from emissions in the Norwegian sector. However, the contribution from British sector is interesting for comparison and was included in the previous report by Semb et al. (1996). In the present calculations of the contribution from emissions in the Norwegian sector to acid deposition and ozone formation, all British emissions were allocated to 50 km × 50 km grid squares. The effect of the British emissions was taken care of as area sources in the EMEP oxidant model, not as point sources.

Due to excessive computer time required, it was not possible to perform model calculations with a large number of Norwegian and British point sources together. The effect of the British emissions was therefore estimated separately, in the same way as for the Norwegian emission sources. A 6 km lumping into megasources was applied for the British individual point sources, as explained for the Norwegian sources. The 20 strongest NO_x emitters among these megasources were calculated with Fotoplume, whereas the rest of the British emissions were taken care of as area sources in the EMEP oxidant model. Table 5 shows the emission numbers for NO_x, CO and VOC from the 20 megasources and all remaining sources (allocated to the grid squares) in the British sector.

Table 5: The emissions from British sector applied in the model calculations, showing the annual emissions from each of the 20 megasources (explained in the text), and the total from all other sources. The x and y indexes refer to the grid numbering given in Figure 3.

Emission source type	No.	x	y	NO_x emissions (tonnes (NO_2)/year)	CO emissions (tonnes CO/year)	VOC emissions (tonnes VOC/year)
Megasources	1	6	17	7997	1805	553
	2	10	10	5074	795	252
	3	9	11	5034	1156	212
	4	8	14	4438	926	209
	5	8	13	4117	1065	433
	6	6	17	4087	792	356
	7	5	17	3874	532	61
	8	6	17	3116	842	851
	9	9	10	2734	790	1779
	10	12	9	2513	610	161
	11	8	11	2445	706	1549
	12	16	2	2423	501	136
	13	5	18	2389	566	127
	14	10	12	2340	543	100
	15	9	12	2227	482	135
	16	17	5	2057	379	109
	17	8	11	1787	309	46
	18	8	11	1782	341	281
	19	6	16	1694	283	41
	20	5	17	1510	386	75
	Sum			**63637**	**13809**	**7465**
Other sources	**Sum**			**25413**	**6249**	**8287**
Total sum				**89050**	**20058**	**15752**

This procedure gives an estimate of the separate contribution from the British emissions if there were no Norwegian emissions in the North Sea. It is difficult to

evaluate if these results will differ significantly from the real situation where the British emissions are transported across and mixed with the Norwegian emissions towards the Norwegian coast. Generally, non-linear effects will reduce the impacts when the NO_x concentrations are high, thus indicating that the present estimation of contribution from British emissions is an upper estimate.

Figure 4 and Figure 5 show the 50 km × 50 km gridded area sources of NO_x and VOC, respectively, excluding the 20 Norwegian megasources. These emission numbers include all British emission, as well as the emissions from shuttle tankers during transport and smaller Norwegian point sources not allocated to the megasources. The emissions from the shuttle ship track to Tranmere at the British west coast are apparent in Figure 4 and Figure 5 as crossing the UK. Although the ship track obviously is very simplified, the emission rates are so small compared to UK's main land emissions, that the small displacement of the ship track is of no importance for the model results.

For comparison Figure 6 and Figure 7 show the NO_x and VOC emissions, respectively, from the 20 Norwegian megasources when allocated to their corresponding 50 km × 50 km grid squares.

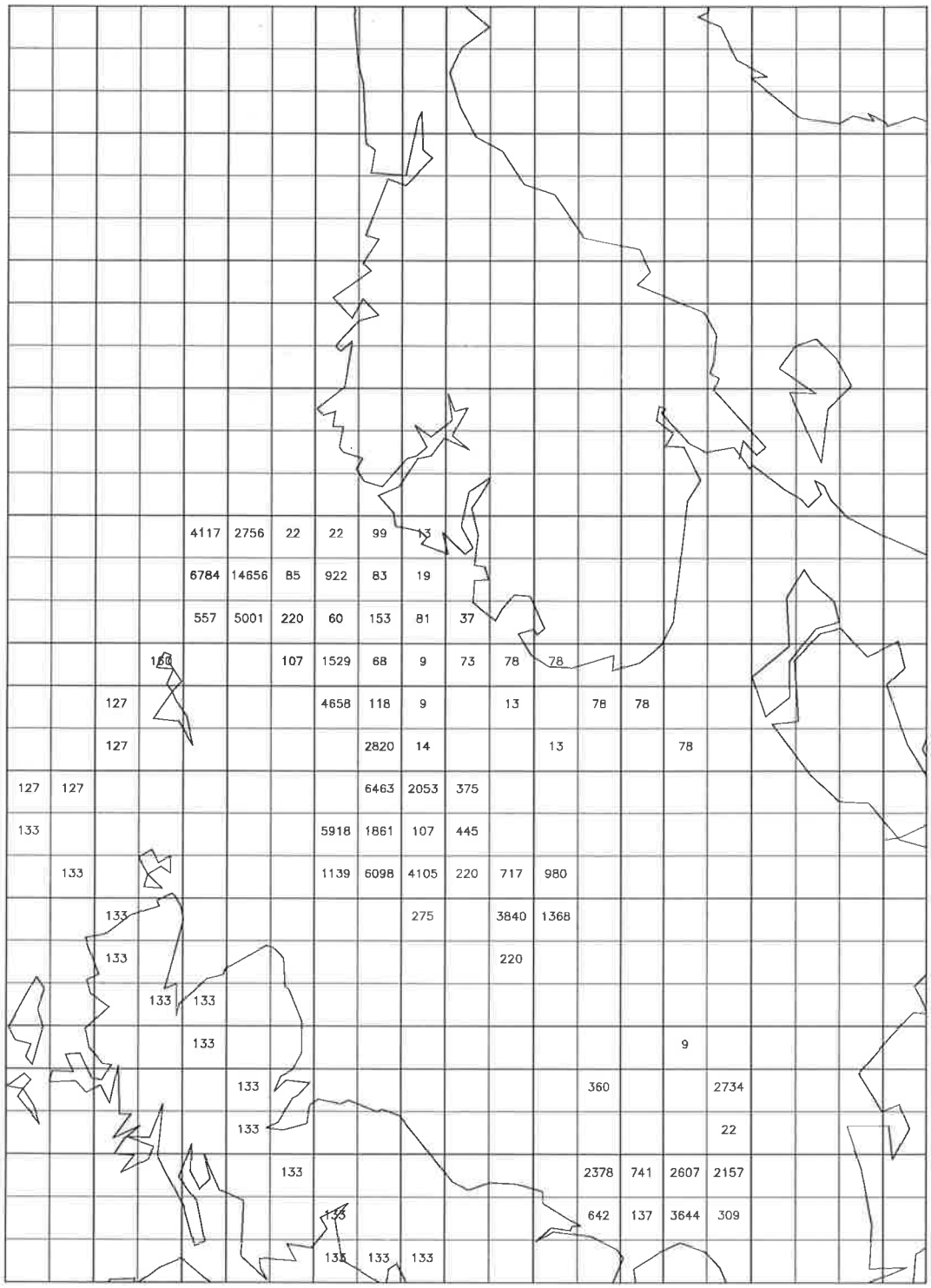

Figure 4: NO_x emissions (tonnes (NO_2)/year) from British and Norwegian petroleum sector, excluding the 20 Norwegian megasources, allocated to EMEP's 50 km × 50 km grid squares.

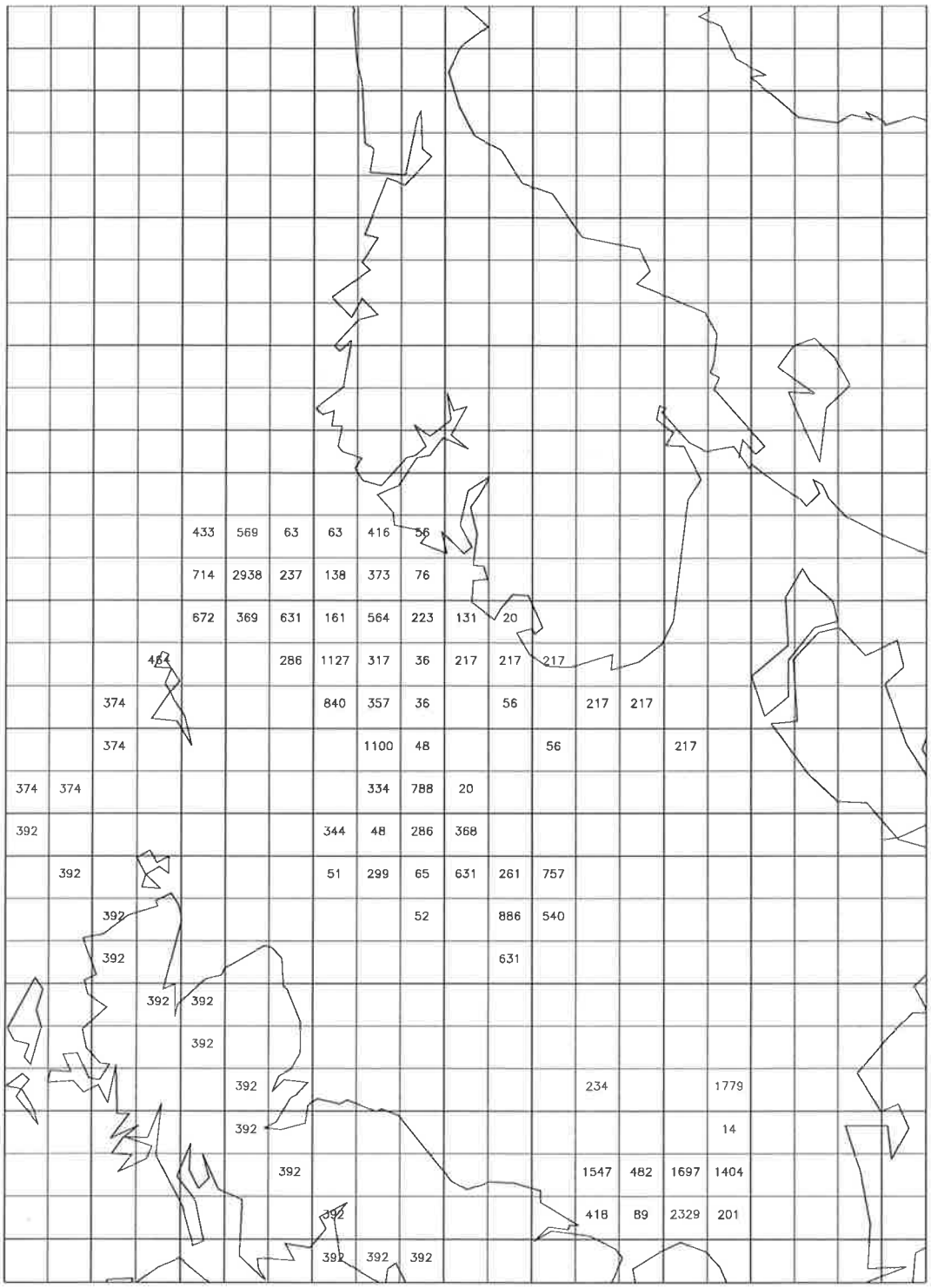

Figure 5: VOC emissions (tonnes (VOC)/year) from British and Norwegian petroleum sector, excluding the 20 Norwegian megasources, allocated to EMEP's 50 km × 50 km grid squares.

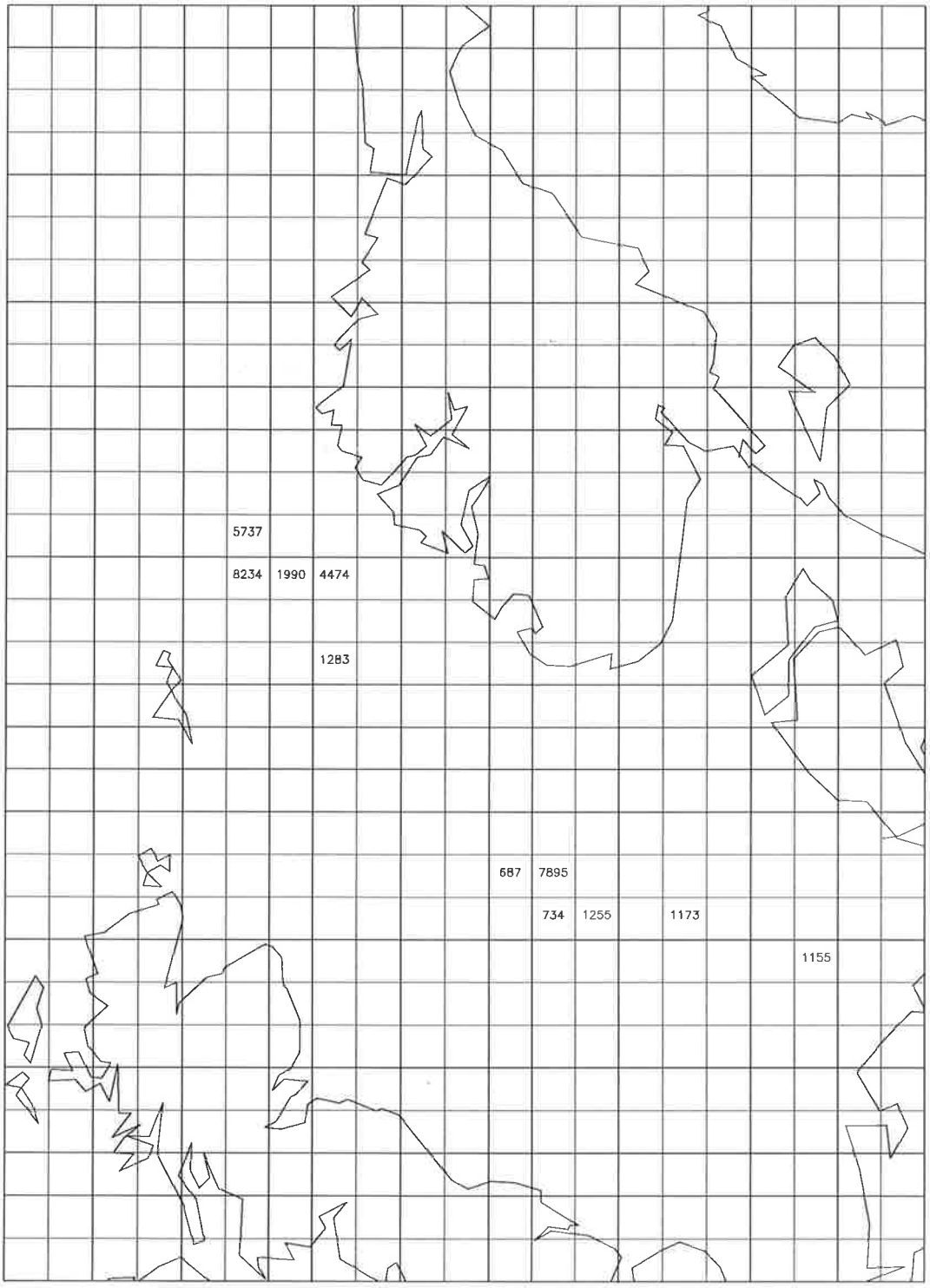

Figure 6: The sum of NO_x emissions (tonnes (NO_2)/year) from the 20 Norwegian megasources, as allocated to the corresponding EMEP's 50 km × 50 km grid squares.

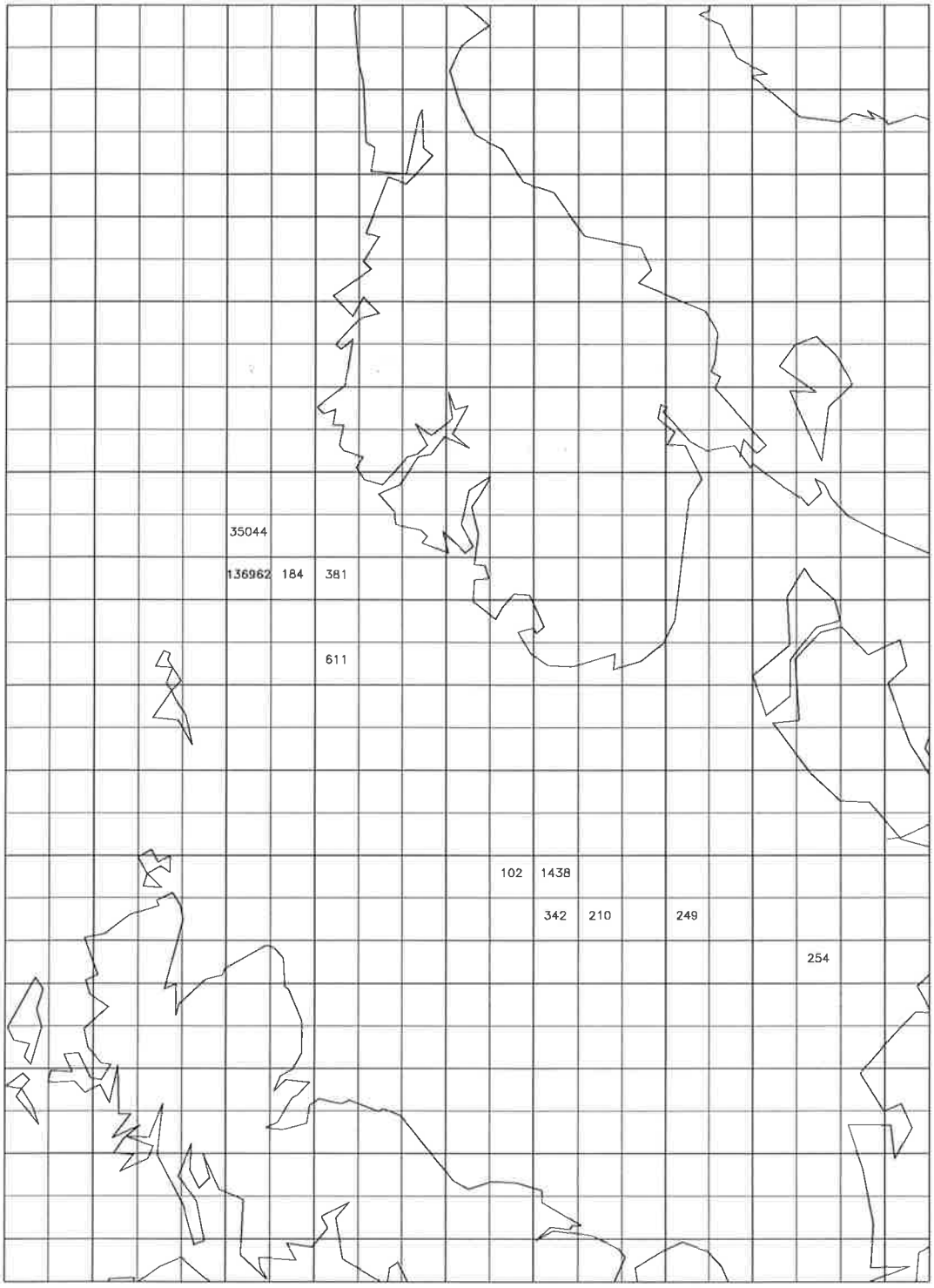

Figure 7: The sum of VOC emissions (tonnes (VOC)/year) from the 20 Norwegian megasources, as allocated to the corresponding EMEP's 50 km × 50 km grid squares.

4. Model description

Several parts of the Fotoplume model have been revised and developed further as part of the current project. Most important is an improved interface to the EMEP trajectory oxidant model and better simulation of the dry and wet deposition processes. In addition a simplified simulation of plume mixing has been included. The model development is described in the following sections.

4.1 The EMEP oxidant model

The EMEP model (Eliassen and Saltbones, 1983; Simpson, 1995) is a one-layer Lagrangian trajectory model which has been developed to describe regional formation and long-range transport of air pollutants in Europe. The model integrates the photochemical reactions for an air parcel following 4 days' trajectories to any receptor points within the EMEP model domain, covering Europe and part of the North Atlantic.

Meteorological data are given each six hours in approximate 150 km × 150 km grid cells on a polar stereographic map (Figure 1). Data for the mixing height are given each 12 hours. Annual emissions are reported by the Parties to the Convention on Long-Range Transboundary Air Pollution. These are given as national totals, but many countries also report emissions in 150 km × 150 km or 50 km × 50 km grids. The Norwegian Meteorological Institute maintains a database of European emission data, and carries out the necessary additional work in estimating annual and diurnal variations, distribution of national total emissions in grid squares, and estimation of missing values. The status of the emission data is given by EMEP MSC-W (1998).

In order to conform with the model formulation, total anthropogenic non-methane hydrocarbons (NMHC) emissions are speciated into equivalent emissions of ethane, ethene, propene, n-butane, o-xylene, formaldehyde, acetaldehyde, methanol and ethanol (Table 3). Natural emissions of volatile organic hydrocarbons are included and represented by isoprene (Simpson, 1995).

The meteorological information is prepared from the international meteorological observational network with the help of the Norwegian Meteorological Institute's numerical forecasting model. The reference height for the meteorological data in the EMEP-model is $\sigma = P/Ps = 0.925$ (i.e. at a surface with an atmospheric pressure of 92.5% of the pressure at the ground). This corresponds approximately to a level 600 m above the ground.

The chemical scheme involves about 70 different compounds, and more than 150 chemical reactions. It has recently been tested against more comprehensive chemical reactions systems, and has been found to simulate adequately both the chemical breakdown of hydrocarbons and the formation of ozone (Kuhn et al., 1997; Anderson-Skold and Simpson, 1999). The model predictions have also been tested against measured concentrations of hydrocarbons and aldehydes at several measurement sites in Europe. Good agreement has been obtained, particularly for aldehydes (Solberg et al., 1995).

4.2 The Fotoplume model

Fotoplume is the name of the photochemical puff-trajectory model developed for OLF with the designated purpose of simulating the effect of the North Sea emissions. Previous versions of the model is presented by e.g. Semb et al. (1996).

Figure 8 shows how the dispersion from a point source is simulated by Fotoplume's stepwise expanding segments. The plume is divided into segments along the mean advection axis. The length of the segments corresponds to the time resolution of this process in the model, presently 30 minutes. Thus, with a mean wind speed of 10 m/s, the segment will be 18 km long. The width and height of the elliptic segments are determined from plume dispersion parameters, which have been taken from the meteorological data. In order to simulate the concentration variations across the plume, each segment is divided into five shells.

The length of the segments is kept constant until they leave the model domain. The width of the segments' shells expand according to Gaussian dispersion theory, thereby entraining air outside the plume into the plume's shells. For the sake of understanding, it is crucial to regard this expansion only as a stepwise change in the 3-dimensional grid encompassing the process (i.e. the plume) we want to study.

This so-called "expansion" does therefore not simulate *any* physical process in the atmosphere, it only reflects that we have to expand the grid in order to keep track of the plume. The true *physical* expansion, i.e. the exchange of gases and particles by turbulent diffusion in the plume (and between the plume and the background air) is modelled separately. This is done by applying diffusion parameters on the interfaces between the shells. The diffusion parameters are calculated from the meteorological data.

When the vertical extension of the plume (or rather *the expanding grid*) has increased to the height of the mixed layer, the shells are replaced by rectangular blocks with a height corresponding to the mixed layer, as shown in Figure 8. This is in accordance with the real situation, where a relatively homogeneous vertical distribution is reached when the plumes are mixed in the whole of the planetary boundary layer.

Concurrently, photochemical reactions are simulated for each segment and shell, with timesteps chosen so that the computational solutions are numerically stable. The photochemical reaction scheme and the reaction rates in Fotoplume are identical with the reaction scheme in the EMEP oxidant model.

The segments are advected with the main wind, which is changed every 6 hours. Because the wind field changes with the location in the EMEP grid, the plumes will travel along curved trajectories. No interpolation of the windspeed or direction is made within the 6-h time intervals.

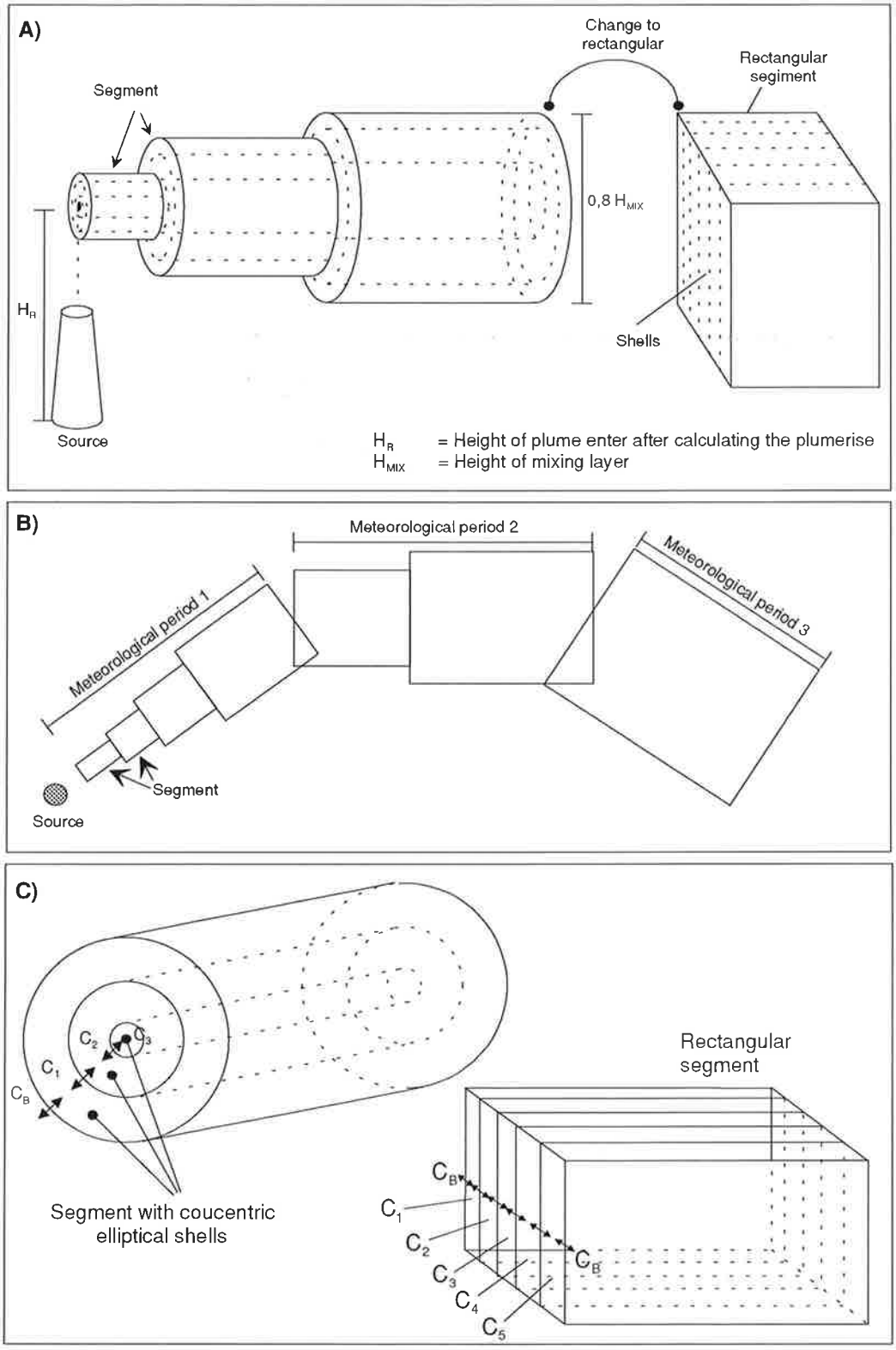

Figure 8: Graphical representation of the dispersion model.
A) The plume segments in perspective.
B) The plume seen from above.
C) One segment with shells.

4.3 The interface between the EMEP trajectory model and Fotoplume

In previous versions of the Fotoplume model, emissions from the underlying 150 km × 150 km EMEP grid squares were not taken explicitly into account, but only indirectly through the use of EMEP background concentrations. This has been changed in the new version of the model in that specially gridded emission fields based on the EMEP 50 km × 50 km grid system are now prepared as input to the model. These emissions are taken into account as soon as the plume segments reaches the ground and are converted into rectangles. For plume segments of ellipsoidal shape, and which have not yet reached the ground, the emissions are set equal to zero as before.

Also concentration fields for the underlying 150 km ×150 km EMEP grid squares (pre-calculated by that model) were previously used as the ambient background concentrations for the plume, and changed as the plume moved from one grid cell into another. Experience showed that this procedure was not ideal, and produced stepwise alterations in the background concentrations due to the six-hourly resolution of the EMEP model. To improve this procedure, a linear interpolation in time is, however, not appropriate as this may result in unrealistic temporal changes in the concentrations. In the new version of Fotoplume, each of the individual plumes are given a surrounding background layer which is following the plume. The background layer is initialised by the EMEP grid square concentration and the concentrations are modified by emissions from the underlying EMEP grid and by chemical reactions in exactly the same way as the main plume.

4.4 Gaussian distribution of initial concentrations

In previous versions of Fotoplume the emissions were distributed uniformly in the initial plume layers. In the new version of the model the emissions are introduced into the plume layers using a Gaussian or normal concentration distribution. This gives a more realistic description of the conditions in the plume initially. It is ensured that the product of concentration and volume added over all plume layers is equal to the total mass emitted during one time step, i.e. that the model is mass-consistent. All other initial plume conditions are taken from the emission database supplied. The necessary parameters include temperature and velocity of the emission, as well as physical dimensions of the initial release. The initial width and height of the plume segments (ellipsoids) is not allowed to be less than 40 m and 20 m respectively in the current version of the model.

4.5 Meteorological pre-processing

NILU's meteorological pre-processor MEPDIM (Bøhler, 1996) is used to generate meteorological data for the Fotoplume model. Input data to the pre-processor is taken from the EMEP meteorological data (150 km × 150 km grid), which is being read into the model every 6 hours of simulation. These data consists of temperature, wind, relative humidity, cloud cover, precipitation, and mixing height. The energy budget method in the pre-processor is used to calculate a vertical wind speed profile and horizontal and vertical turbulence intensities using 10 vertical layers from the ground and up to 1000m. This method calculates the energy balance between air and sea/land from the given cloud cover, fluxes of sensible and

latent heat and the net radiation. The energy balance is subsequently used to calculate the turbulence intensities in the atmosphere.

The reference height for the meteorological data in the EMEP-model is $\sigma = P/Ps = 0.925$ (i.e. at a surface with an atmospheric pressure of 92.5% of the pressure at the ground). This corresponds approximately to a level 600 m above the ground.

The surface roughness is set equal to 0.01 m over sea and 0.3 m over land. The albedo is set equal to 0.2 in both cases. The cloud cover is taken directly from the EMEP meteorological data.

Wind speeds and horizontal turbulence intensities, σ_v, is calculated in the midpoints of each vertical layer using reference heights of 50 m, 150 m etc. up to 950 m in steps of 100 m above sea level or ground. Vertical turbulence intensities, σ_w, is calculated using reference heights equal to the top of each vertical layer, i.e. at 100 m, 200 m etc. up to 1000 m. The same pre-processor was also used previously, but with a much coarser vertical resolution using only three layers.

4.6 Deposition calculations

In the calculations reported previously by Semb et al. (1996) the dry and wet deposition of nitrogen was only performed as a post-processing calculation based on the calculated atmospheric concentrations of nitrogen species. One of the important aims of the present model development was to include deposition calculations in the Fotoplume model.

In the present version of the model wet and dry deposition processes have been included in the model. The process simulation has been adopted from the EMEP trajectory oxidant model (Simpson, 1995). This has furthermore improved the interface and the comparability of the calculations of these two models.

Wet deposition of oxidised nitrogen species are most effective for nitric acid (HNO_3) and particulate nitrate (NO_3^-), and small for other nitrogen compounds. Wet deposition is a very complex physical and chemical process at the micro level, and could be calculated in an extremely detailed manner on a droplet basis. For regional scale models the processes have to be simplified. The description adopted from the EMEP model into Fotoplume, uses the parameterization:

$$dc/dt = - (\Lambda P/H)\, c$$

where

dc/dt is the time derivative (loss rate) of the compound
Λ = scavenging ratio
P = precipitation rate
H = height of the planetary boundary layer.

Λ is set equal to $1.4 \cdot 10^6$ for HNO_3 and $1.0 \cdot 10^6$ for nitrate particles as in the EMEP model.

Precipitation data in the Fotoplume model is taken from the EMEP meteorological data that has a horizontal resolution of 150 km × 150 km and a temporal resolution of 6 hour. On the western coast of Norway however, the precipitation pattern is very much dependent upon the topography. When the wind direction is towards land the air masses will be elevated and there is much higher probability of precipitation. This gives local precipitation patterns on the western coast of Norway with large variations over a much finer scale than reflected in the 150 km scale of the EMEP data. Furthermore, precipitation is a crucial parameter in the calculation of wet deposition of nitrogen.

In the new version of Fotoplume EMEP's 150 km scale precipitation data is scaled to a 50 km scale by taking into account existing data for annual precipitation in 50 km × 50 km grid squares for Norway. The precipitation rates in EMEP's 150 km × 150 km grid is scaled each six hour in each 50 km × 50 km grid square by the factor expressing the relative factor of the 50 km and 150 km grid squares annual precipitation amount. This implies that we assume that the relative precipitation pattern inside each 150 km × 150 km grid cell is identical at all times. This we admit is a simplification, as it will vary with season and the type of precipitation (convective or orographic). Ideally this scaling should also take into account seasonal effects, and be performed on e.g. a monthly basis. The 50 km precipitation data were, however, only available as annual totals.

Parameterization of dry deposition has also been introduced in the Fotoplume model. The dry deposition rate for ozone and nitrogen dioxide are mainly controlled by the diffusion resistance through the plant's stomata. This deposition therefore depends on the ground cover and season. The uptake to snow covered surfaces are negligible.

For HNO_3 the dry deposition rate are mainly controlled by the aerodynamic resistance, which give deposition rates in the order of 2-5 cm/s relative to a height of 2-10 m, sometimes even higher (Dollard et al., 1987; Meixner et al., 1987). Snow covered surfaces are exceptions to this, showing negligible deposition at temperatures below -2°C (Johansson and Granat, 1982). For a situation with relatively strong winds and neutral stability, the aerodynamically resistance is given by the following expression:

$$r_a = \frac{u}{u_*^2} = \frac{\left(\ln z/z_0\right)^2}{k^2 \cdot u}$$

The surface roughness (z_0) over sea is typically a few mm, about 0.1 m over agricultural land, and typically somewhat less than 1 m in forests.

To take into account the vertical profile of the components, it is common to use a constant flux approximation, where the basic idea is expressed as:

$$(v_d c)_{50m} = (v_d c)_{1m}$$

where v_d is the dry deposition rate and c is the concentration.

A dry deposition rate appropriate for 50 m is then calculated by the expression (Eliassen and Saltbones, 1983):

$$v_{d_{50m}} = v_{d_{1m}}/[1 + v_{d_{1m}}(r_a(z=50m) - r_a(z=1m)]$$

where r_a is the aerodynamic resistance

This parameterization is included in the Fotoplume model, and the dry deposition rates (vd_{1m}) were adopted from the EMEP model. The dry deposition velocities depend to a large extent upon whether we are over land or over sea. In the new version of Fotoplume land/sea indicators were introduced with the 50 km × 50 km resolution.

4.7 Mixing of plumes

In previous versions of the Fotoplume model, individual plumes from different sources did not interact, i.e. the diffusion calculations for each individual plume segment was performed using only the atmospheric background concentrations and did not take into account possible influences by other nearby plumes. The goal of the current work was to include such a general diffusion or mixing of plumes as part of the Fotoplume model. However, this has proved to be more difficult than first anticipated.

As long as there are only two plume segments which interact it is possible to calculate the effects that each of these plumes may have on each other. However, since the Fotoplume model, in general, calculates on a large number of plume segments, and for an arbitrary set of point source positions, there will inevitably be many cases with a large number of overlapping plume segments. Added to this complexity is the large number of different 3-dimensional geometrical situations which may arise. In reality it therefore seems an impossible task to keep track of the way different plume segments may influence other plume segments using this Lagrangian framework without any constraints. A detailed simulation of plume mixing would require a combined Eulerian/Lagrangian model, outside the scope of the present model development.

A simplified procedure for simulation of plume mixing was, however, included in the new version of the model, and is described below. This procedure handles mixing of pairs of neighbouring plumes. When three or more plumes interact, the complexity increases substantially, and is not solved by the present approach.

In addition, we note that the improved handling of individual emission sources, using the new procedure for generating megasources, as explained above, also partly solves the problem of plume mixing. This method has reduced the number of modelled sources considerably and improved the spatial separation between the sources.

4.7.1 Asymmetrical rectangles

As long as a plume is not influenced by any other plume, the plume will remain symmetrical, i.e. the widths on both sides of the centreline will be equal. When

plumes are allowed to interact it is important to stop the Gaussian expansion of the grid, as defined in section 4.2. If this is not done, different segments may begin to overlap spatially which is detrimental to the concept of plume interaction. The idea is instead that each segment should describe in a unique manner that part of the atmosphere for which its volume occupies.

Therefore, asymmetrical plume rectangles are introduced in the new model version. This means that the left part of a rectangle may have a different width than the right part of the rectangle. As soon as a plume is influenced by another plume, the Gaussian grid expansion of the two rectangles will be stopped at the intersecting side. It remains so until the two plumes are transported out of the model domain.

All kinds of geometrical plume mixing may occur. In the Fotoplume model, these are sorted into two classifications, *one-way* diffusion or *two-way* diffusion, as described below.

4.7.2 One-way diffusion

If a plume segment (either ellipsoid or rectangle) is much smaller than the other plume segment it encounters (or is contained in the other plume segment), there will be a *one-way* diffusion. The larger plume segment will have an effect through diffusion on the smaller plume segment, but the smaller plume segment will have negligibly effect on the larger plume segment.

Numerically one-way diffusion needs only be solved for the smaller of the two plume segments, using concentrations from the larger plume segment as boundary condition for the diffusion operator. The larger plume segment in this case is still free to participate in other kinds of one-way or two way diffusion interactions.

4.7.3 Two-way diffusion

Two-way diffusion arises when two intersecting plume segments (either ellipsoids or rectangles) are of comparable size. In this case it is impossible to maintain the assumption of concentration isocurves of ellipsoidal shape so both are converted to rectangles. If the directions of the two plume segments are not the same, they are rotated so that both rectangles point in the same direction. Usually this rotation is small. The rectangle lengths and heights will not be adjusted but different cross-section areas are taken into account in the formulation and solution of the diffusion equation.

Numerically, two-way diffusion is solved for both plume segments simultaneously, using background concentrations for one of the plumes on one side and background concentrations for the other plume on the other side. The plume segments will exchange mass by this process through a common border between the two plume segments. The complete process is mass consistent since the diffusion process only implies an exchange of mass between the two rectangles.

4.8 Procedure of model calculations

The aim of the project was to estimate the contribution of emissions from the petroleum activity in the Norwegian sector of the North Sea to nitrogen

deposition and ozone exposure in South Norway. This contribution will be an addition to the influence imposed by the overall European emission of NO_x and VOC. This implies that the incremental addition from the North Sea should be estimated very carefully to separate the real effect from "noise" resulting from uncertainties in the model formulation.

The calculations were performed with a combination of two types of numerical models: a) A regional Lagrangian (trajectory) model (the EMEP oxidant model) and b) the point source model Fotoplume, developed further during this project. The trajectory model can be used for calculations to any number of selected receptor points within the underlying EMEP grid. LPSs (Large Point Sources) are not handled by this model, instead all emissions are smoothed to a specified minimum grid resolution, currently 50 km × 50 km. This is acceptable for relatively homogeneous emissions fields or in situations when the source-receptor relationship is fairly linear. For a situation as the North Sea, dominated by a number of distinct point sources not too far from the influence area in South Norway the smoothing induced by a 50 km resolution will give rise to shortcomings and unreliable results.

The procedure of model calculations performed with the new version of Fotoplume is shown in Table 6. These model calculations were performed for 1992 as well as 1995, i.e. with meteorology for 1992 and 1995 (but with the same emissions).

Table 6: Procedure of model calculations.

E_0	EMEP excluding all of the North Sea
E_B	EMEP with British sector
E_N	EMEP with British sector and Norwegian area sources
F_N	Fotoplume with Norwegian megasources initialised by E_N
F_{N0}	Fotoplume with Norwegian megasources with zero emissions intialised by E_B
F_B	Fotoplume with British megasources initialised by E_0
F_{B0}	Fotoplume with British megasources with zero emissions intialised by E_0

The contributions from Norwegian (N) and British (B) sectors were then calculated according to the following expressions:

$$N = F_N - F_{N0}$$
$$B = F_B - F_{B0}$$

These symbols refer to the annual numbers in each receptor point for dry and wet deposition of nitrogen as well as the AOT40 for ozone exposure.

The procedure for calculating the contribution from the Norwegian sector is explained as the following: First two runs with the EMEP trajectory model were made, with and without the Norwegian area sources, respectively (and without the megasources). Then the Fotoplume model was run twice, first with real emission

data for the megasources and initialised by the results from the EMEP model including Norwegian area sources. Secondly, Fotoplume was run with emissions set equal to zero and initialised by the results of the EMEP model excluding the Norwegian area sources. The difference between these two sets of Fotoplume calculations then expresses the contribution to nitrogen deposition and ozone exposure from the Norwegian North Sea emissions. This rather elaborate procedure was used to minimize the effect of uncertainties in model performance between the EMEP and Fotoplume model.

The AOT40 calculations for ozone are by definition very sensitive to the absolute level of ozone. A relative difference in the ozone concentration of, say 10%, may have a large impact on the calculated AOT40. For the AOT40 calculations it is therefore important to take into account the diurnal cycle in ozone which arises due to the surface removal and which is apparent from the observations but not well reproduced in a regional scale model. The reason for this is that the surface removal depends on very local conditions (topography, land use etc.). As the modelled AOT40 values are to be compared with the measured values, the calculated ozone concentrations were not used directly in the AOT40 calculations. Instead a spatially interpolated observational field (interpolated every hour throughout the year) was scaled according to the change in two sets of model calculations:

$$O_{sce} = O_{ref} \cdot M_{sce}/M_{ref}$$

where

O_{sce} = Estimated hourly ozone concentrations for one emission scenario.
O_{ref} = Hourly ozone observations interpolated to all receptor points.
M_{sce} = Modelled hourly ozone concentrations for one emission scenario.
M_{ref} = Modelled hourly ozone concentrations for the reference scenario.

This procedure and the interpolation routines are identical to the ones used in a recent project for the State Pollution Authority (SFT) in Norway, with the aim of calculating crop loss due to ozone exposure (Tørseth et al., 1998).

5. Results

5.1 Nitrogen deposition

The calculations have been performed for two complete years, 1992 and 1995 to evaluate the differences due to meteorological situations. Note that the same emission data (valid for 1992) were used for both the 1992 and 1995 calculations. Thus, the results calculated for 1995 are not really representative for the North Sea contribution that year and should only be used to evaluate the effect of different meteorology from one year to another. Figure 9 shows the observed N-deposition fields for 1992 and 1995, respectively. These values give the total sum of wet and dry deposition of oxidised (HNO_3 + NO_3^-) and reduced (NH_3 + NH_4^+) nitrogen in each grid square. The wet deposition fields are based on measured wet deposition at a number of monitoring sites together with measured precipitation at a large number of stations.

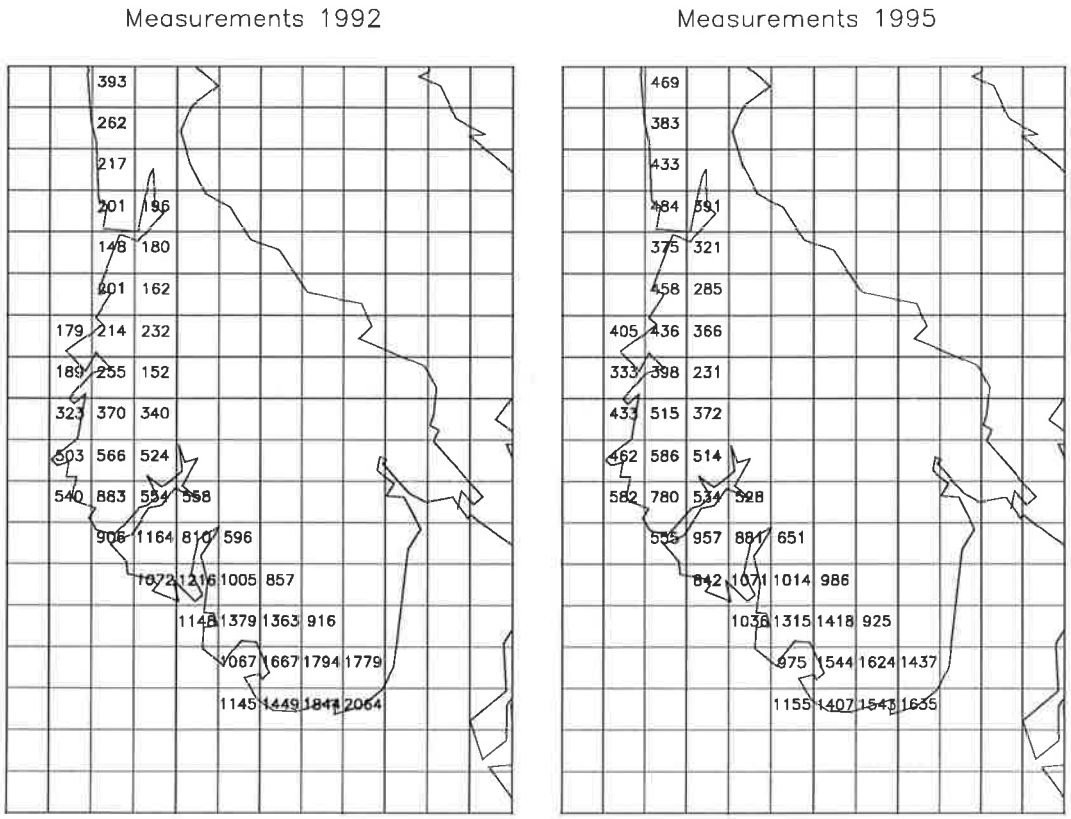

Figure 9: Total deposition of nitrogen (mg (N)/m²) in the receptor grid squares in 1992 and 1995 based on measured wet deposition of N and measured atmospheric concentrations of nitrogen species and assumed dry deposition rates.

The dry deposition are not measured directly, instead the "observed" dry deposition are inferred from daily observed atmospheric concentrations of nitrogen compounds and assumptions regarding the deposition rates.

It is furthermore important to beware that the emissions from the petroleum industry only contributes to the deposition of *oxidised* nitrogen (NO_x, NO_3^-, etc.), whereas the observation fields shown in Figure 9 is the sum of oxidised and reduced nitrogen deposition. Deposition of *reduced* nitrogen ($NH_4^+ + NH_3$) is mainly due to ammonia emissions from agriculture. For the harmful effects, however, it doesn't matter whether the nitrogen is in reduced or oxidised form. In Southern Norway reduced nitrogen contributes slightly less than half (about 40%) of the total nitrogen deposition shown in Figure 9.

Figure 10 shows the calculated absolute and relative contribution from Norwegian and British sector to the total N-deposition in 1992. Figure 11 and Figure 12 shows the contribution to the wet and dry deposition of oxidised nitrogen from Norwegian and British emissions in 1992, respectively. The results from the calculations with 1995-meteorology are shown in Figures 13-15.

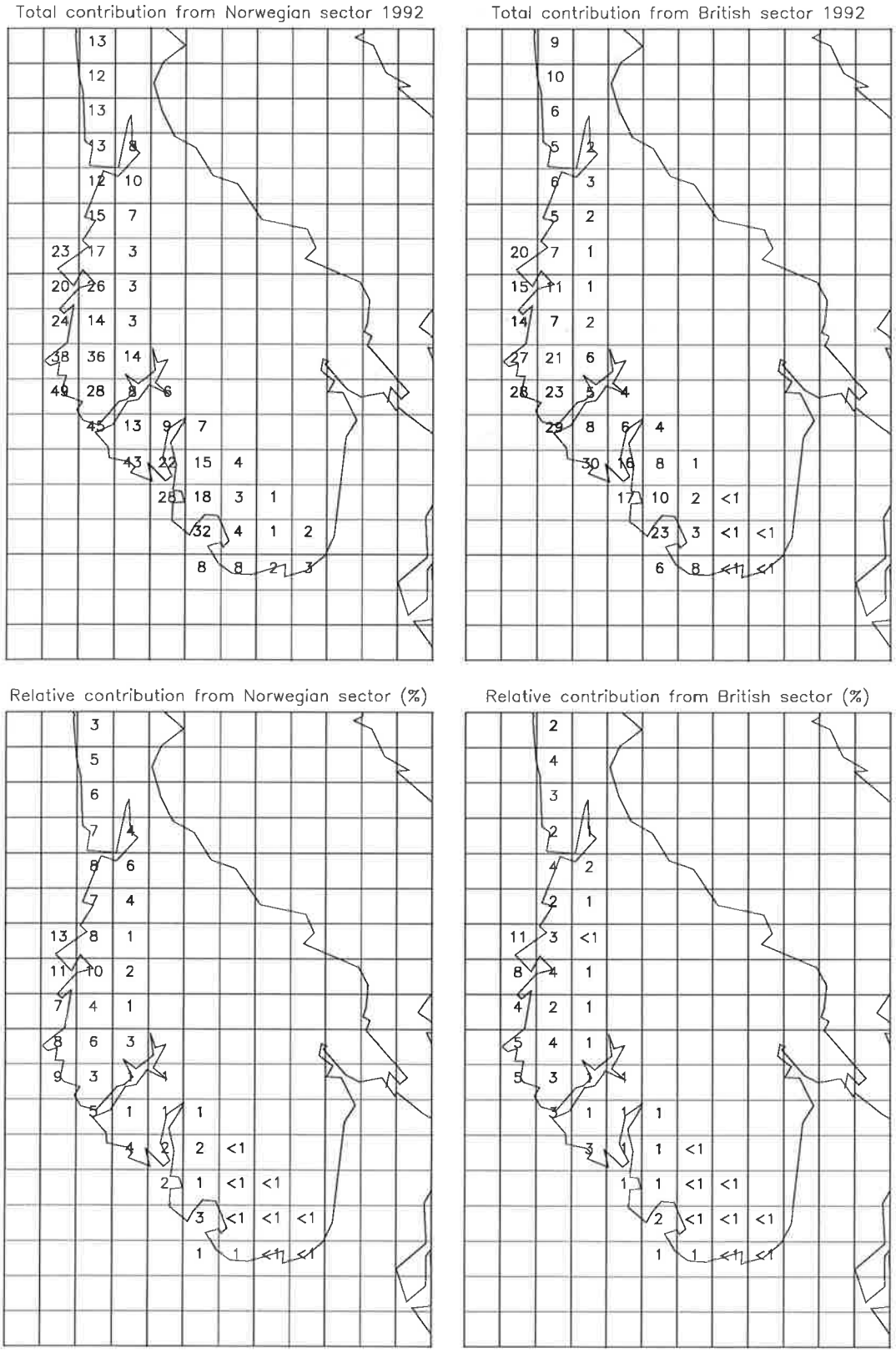

Figure 10: Calculated contributions to the N-deposition in the receptor grid squares from Norwegian sector (left) and British sector (right) in 1992. The upper row gives the absolute contribution (mg (N)/m²) and the lower row gives the contribution relative to the observed deposition.

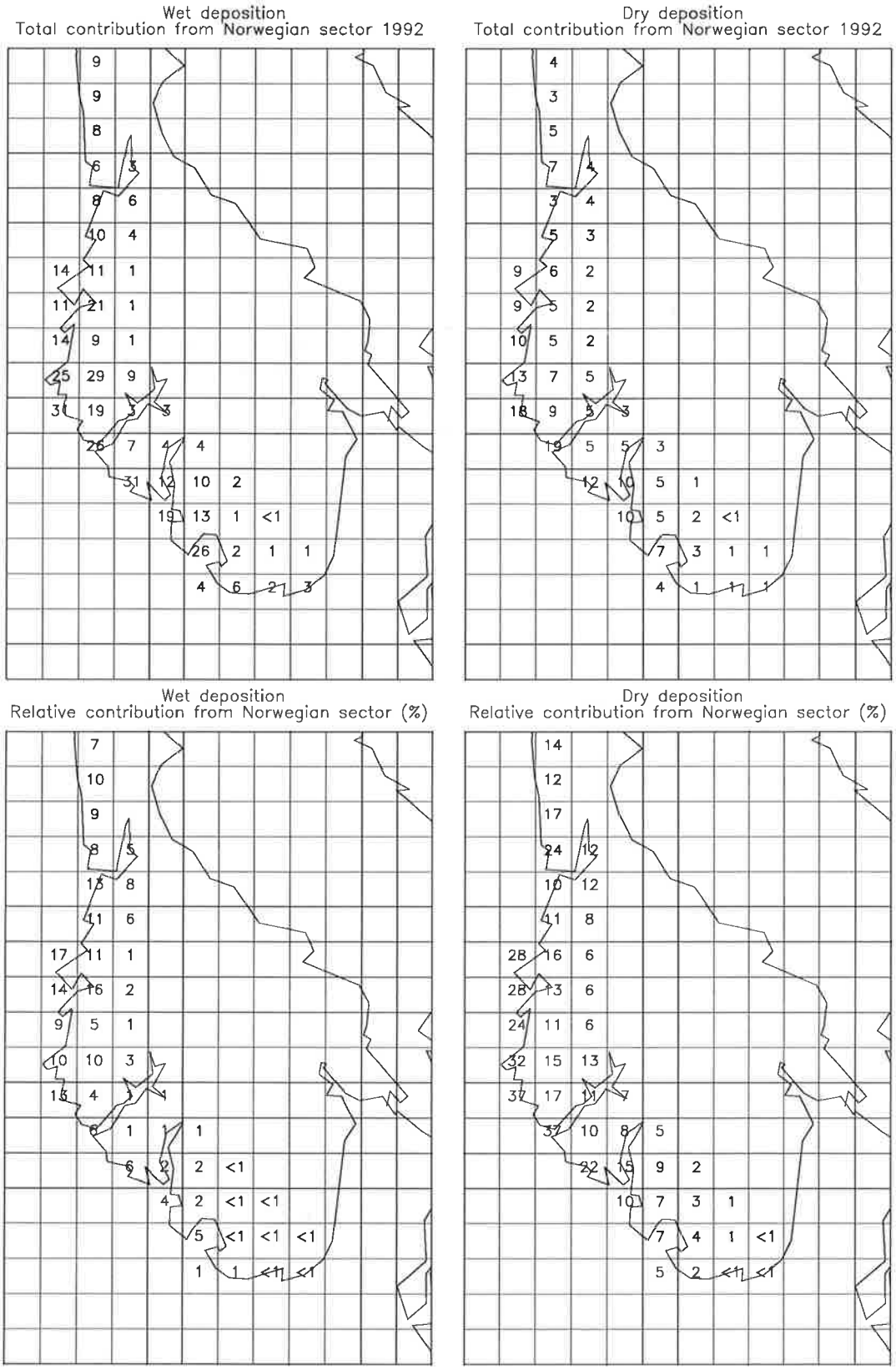

Figure 11: Calculated contributions to the wet (left) and dry (right) deposition of oxidised nitrogen in the receptor grid squares from Norwegian sector in 1992. The upper row gives the absolute contribution (mg (N)/m²) and the lower row gives the contribution relative to the observed deposition.

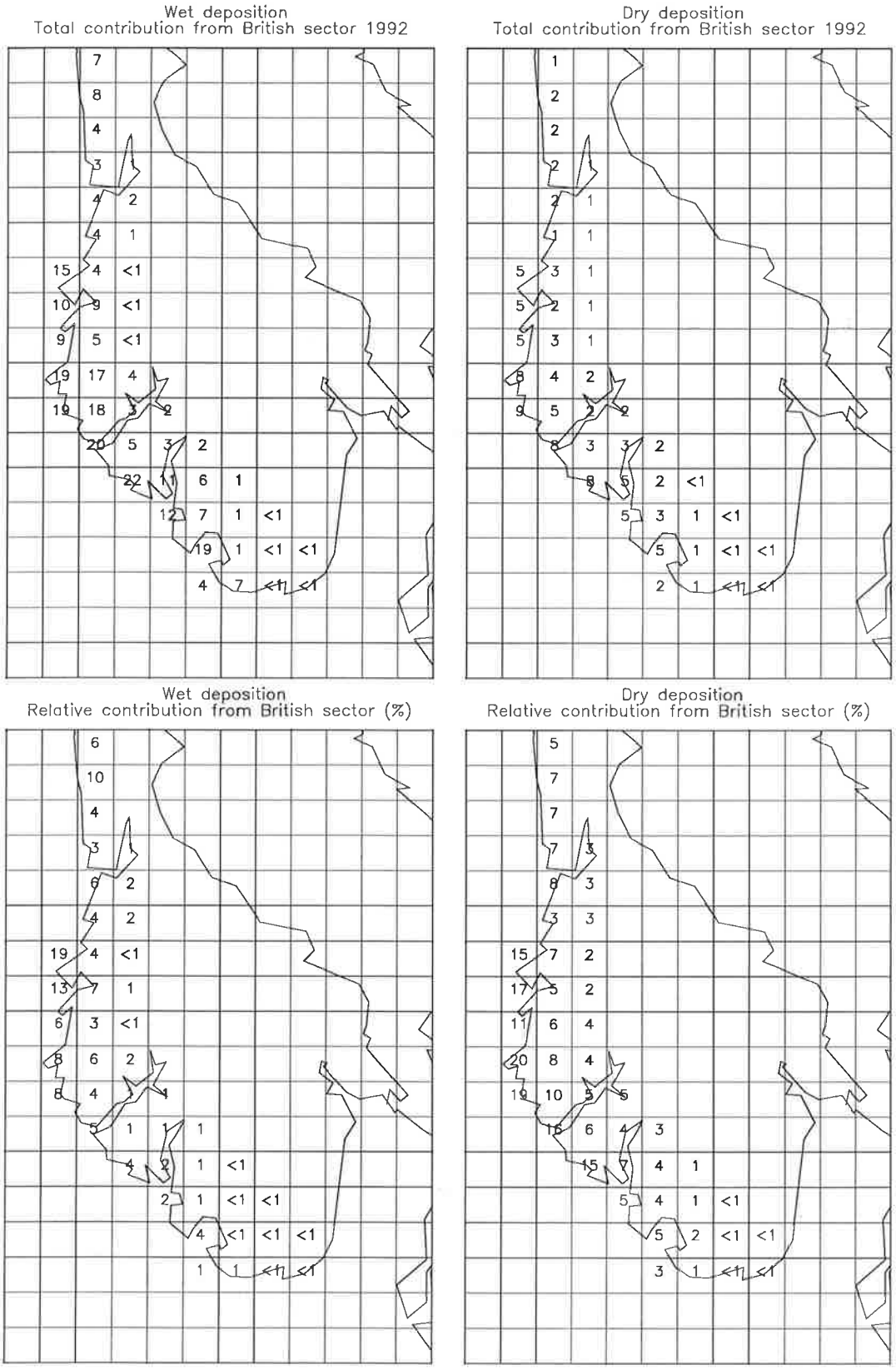

Figure 12: Calculated contributions to the wet (left) and dry (right) deposition of oxidised nitrogen in the receptor grid squares from British sector in 1992. The upper row gives the absolute contribution (mg (N)/m²) and the lower row gives the contribution relative to the observed deposition.

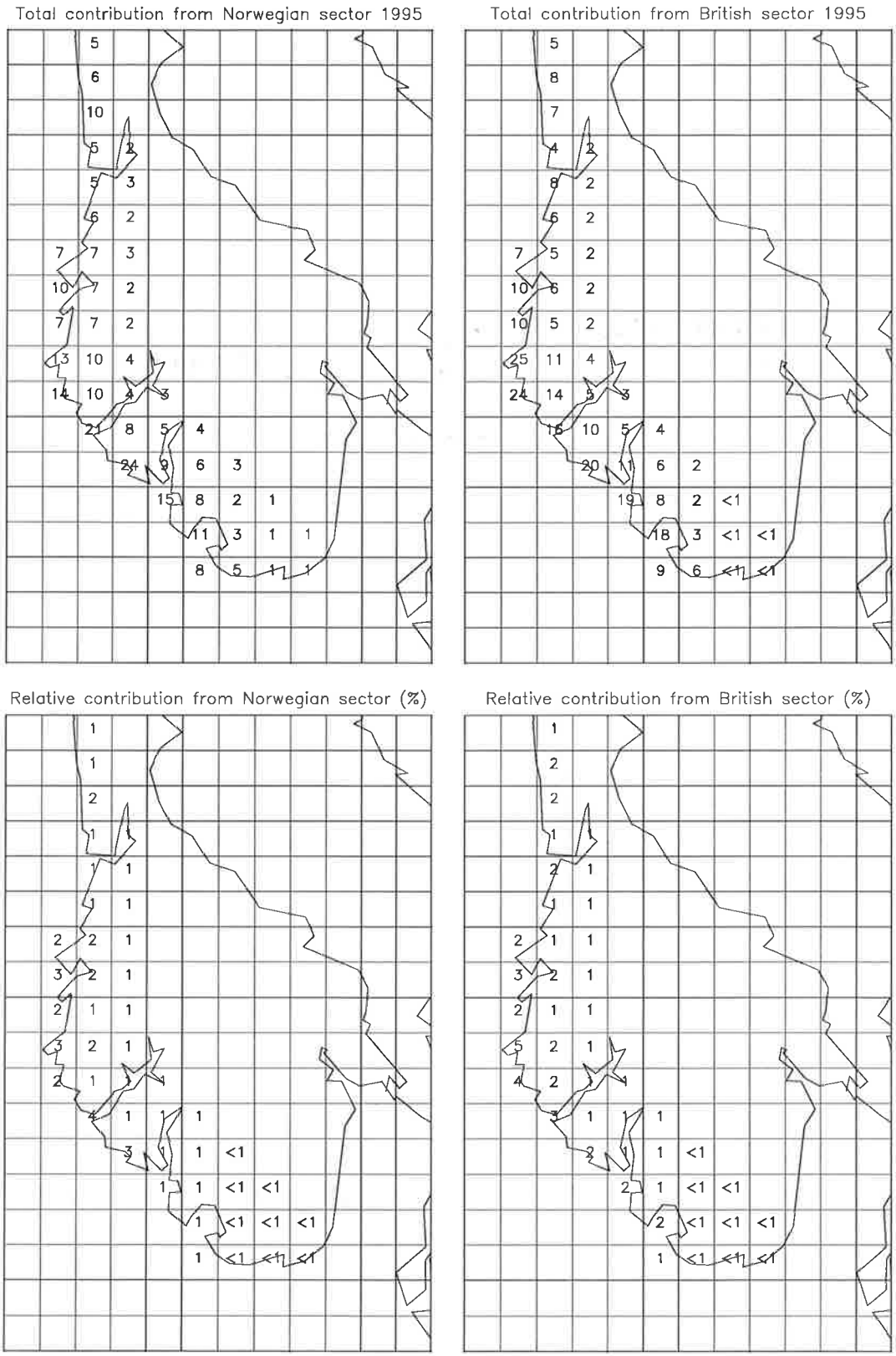

Figure 13: Calculated contributions to the N-deposition in the receptor grid squares from Norwegian sector (left) and British sector (right) in 1995. The upper row gives the absolute contribution (mg (N)/m²) and the lower row gives the contribution relative to the observed deposition.

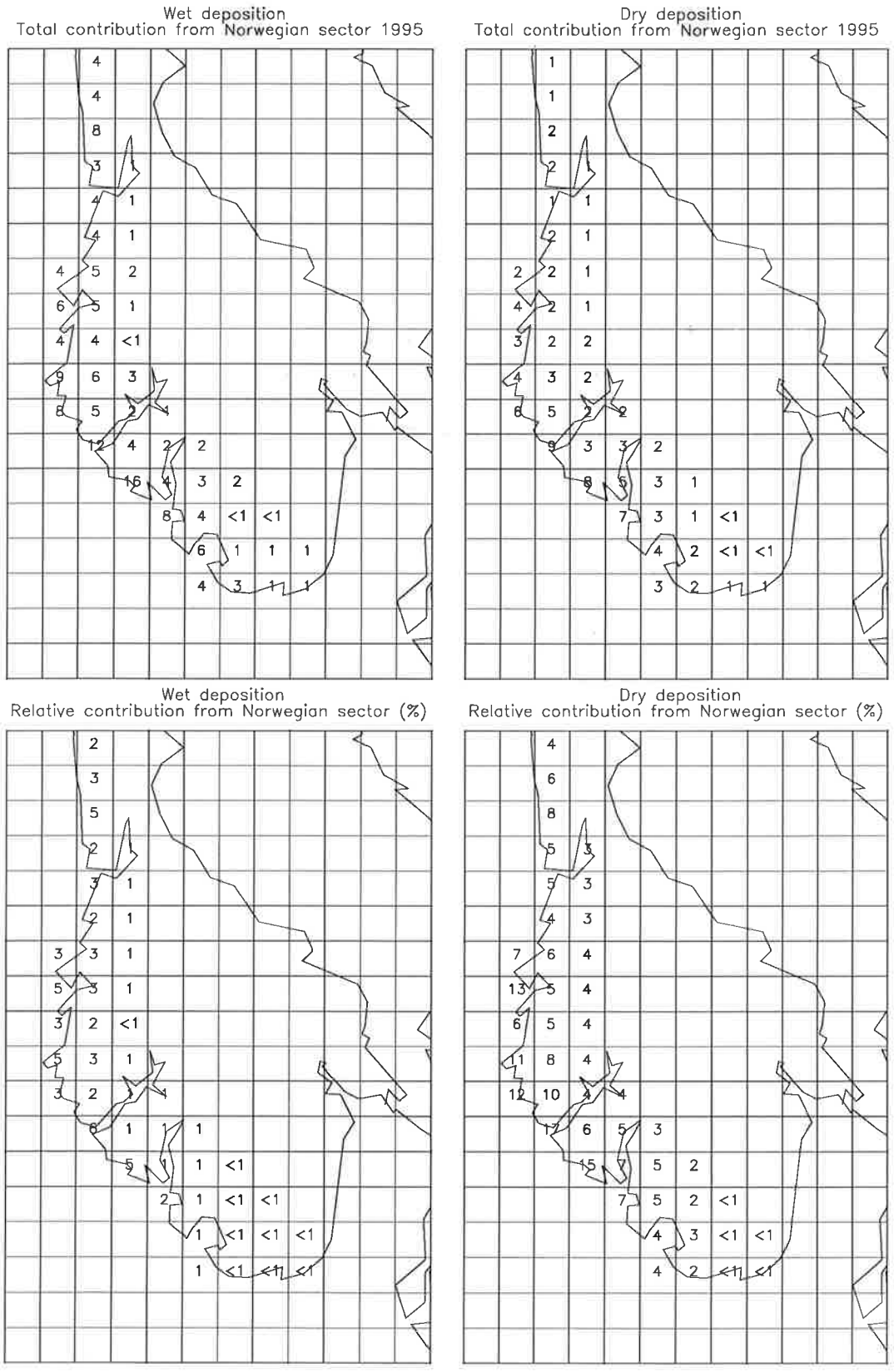

Figure 14: Calculated contributions to the wet (left) and dry (right) deposition of oxidised nitrogen in the receptor grid squares from Norwegian sector in 1995. The upper row gives the absolute contribution (mg (N)/m²) and the lower row gives the contribution relative to the observed deposition.

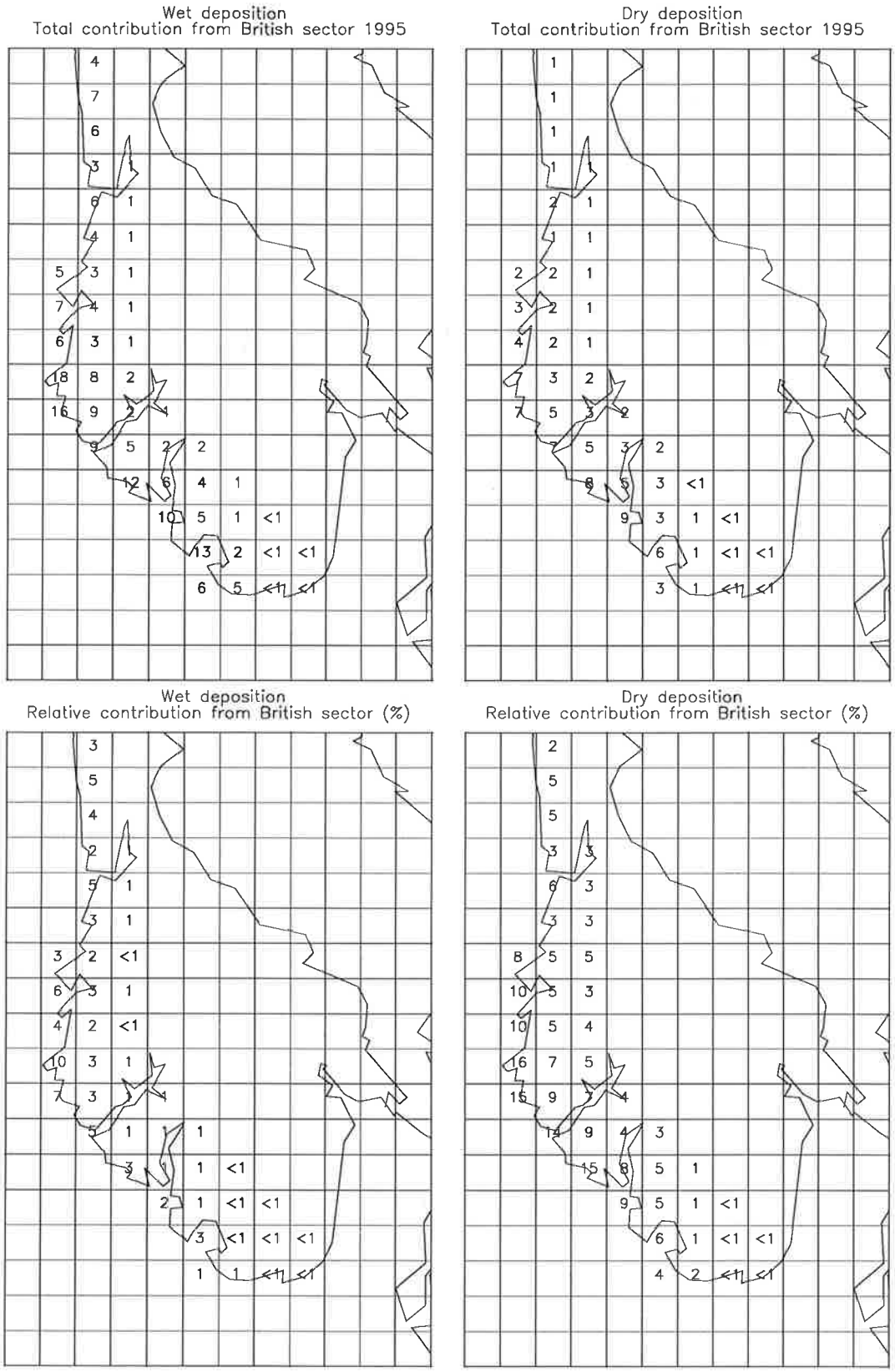

Figure 15: Calculated contributions to the wet (left) and dry (right) deposition of oxidised nitrogen in the receptor grid squares from British sector in 1995. The upper row gives the absolute contribution (mg (N)/m²) and the lower row gives the contribution relative to the observed deposition.

It should be noted that the fields based on the observations are not necessarily correct in all details. The observational fields are interpolated from a few monitoring sites for air and precipitation chemistry, which are then interpolated geographically according to the monitoring of precipitation and the surface cover classification. The monitoring of precipitation amount (from the Norwegian meteorological institute, DNMI) and the ground cover classification have a fairly good spatial resolution, but the chemical monitoring sites include only about 5-10 in the influence area, and small-scale variations may therefore be lost (not detected) in this coarse network.

As shown by Figure 9, the measured nitrogen deposition increases substantially from 200-400 mg (N)/m^2 (or even less) in Trøndelag to 2000 mg (N)/m^2 in southern Norway (in 1992).

The calculated total contribution from the North Sea in 1992 show maxima of 40-50 mg (N)/m^2 and 20-30 mg (N)/m^2 in the coastal areas of Hordaland and Sogn og Fjordane for Norwegian and British sectors, respectively, as shown in Figure 10. This makes a total contribution of 60-80 mg (N)/m^2 from the petroleum activity in the North Sea in this region. The largest *relative* contribution from the North Sea is further north, in Møre og Romsdal, with maximum values of 10-13% for each of Norwegian and British sector compared to the total nitrogen deposition in 1992 (including both oxidised and reduced nitrogen). This totals approximately 20% of the measured deposition in this region. The calculations give a marked maximum zone in N-deposition from the North Sea emissions along the coast, whereas the calculated deposition drops inland. The calculations indicate only a minor contribution from the North Sea emissions to N-deposition in the most exposed areas in the southern part. The calculated total contribution to the N-deposition in Agder is less than 10 mg (N)/m^2 from each of Norwegian and British sector, separately.

The receptor points were allocated to their respective counties and this allocation was used to estimate average deposition values for the separate counties. The results for 1992 are shown in Table 7. As this is a very crude approach, the results in Table 7 should only be used to compare the results for the different counties, and should not be taken as a detailed calculation for the county-wise N-deposition.

Table 7: Estimated average N deposition in counties from the measurements and the calculated contributions from the Norwegian and British sector of the North Sea in the receptor points in 1992. Unit: mg (N)/m².

	Measurements	Contribution from Norwegian sector	Contribution from British sector
Vest-Agder	1679	2	< 1
Rogaland	1275	11	8
Hordaland	1002	20	13
Sogn og Fjordane	609	24	15
Møre og Romsdal	262	18	11
Sør-Trøndelag	173	10	4
Nord-Trøndelag	267	11	7

Figure 11 shows the calculated results for 1992 in more detail, i.e. split into the wet and dry deposition, separately, for emissions from the Norwegian sector. These results indicate that the wet deposition of the Norwegian North Sea emissions is larger than the dry deposition in most of the influence region. Compared to the observed wet and dry deposition of oxidised nitrogen, however, the calculations indicate that a substantial fraction of the observed oxidised dry deposition (up to 30-40%) stems from emissions in the Norwegian sector, whereas at most 10-15% of the oxidised wet deposition stems from the Norwegian sources. The same pattern is also seen for the calculated contributions from British sector, as shown in Figure 12.

This has a physical explanation. The wet deposition, i.e. rain-out in precipitation, is effective only for HNO_3 and not for NO_2 and thus requires a sufficient processing time for oxidation of the original NO_x emissions to HNO_3. The dry deposition, on the other hand, is effective for NO_2, as for HNO_3, and may thus contribute close to the emission sources, as no time is needed for chemical processing in the atmosphere. Besides, closer to the sources the NO_x concentration is higher and dry deposition of NO_2 could then contribute significantly.

The calculated contributions from the North Sea to the nitrogen deposition, using 1995-meteorology, shown in Figure 13, gives in general significantly lower deposition values, as compared to 1992. This regards particularly the contribution from Norwegian sector. The maximum total N-deposition is calculated to be 20-25 mg (N)/m² for emissions from each of Norwegian and British sector in 1995. With 1995-meteorology the maximum area of influence from the Norwegian sector is displaced somewhat to the south. The geographical pattern of N-deposition of North Sea emissions in 1995 is, however, rather similar the one calculated for 1992. The calculations give a maximum deposition zone along the coast in 1995 as in 1992. Only minor deposition is calculated in Agder and in the most inland areas in 1995. An estimation of the county-to-county differences in the N-deposition with meteorology for 1995, similar to that for 1992, is given in Table 8.

Table 8: Estimated average N deposition in counties from the measurements and the calculated contributions from the Norwegian and British sector of the North Sea in the receptor points using 1995-meteorology. Unit: mg (N)/m².

	Measurements	Contribution from Norwegian sector	Contribution from British sector
Vest-Agder	1433	1	< 1
Rogaland	1257	6	7
Hordaland	922	10	11
Sogn og Fjordane	556	8	10
Møre og Romsdal	404	7	8
Sør-Trøndelag	366	4	4
Nord-Trøndelag	419	6	6

Figure 14 and Figure 15 (which are equivalents to Figure 11 and Figure 12, but for 1995) indicate that the lower deposition contribution from the North Sea calculated for 1995 is due to reductions in both the wet and dry depositions compared to 1992. This probably reflects that the meteorological transport pattern and the atmospheric oxidation is decisive for the deposition of North Sea NO_x emissions. As soon as the meteorology carries plumes from the North Sea to the Norwegian coast, dry and wet deposition will both occur due to the probability of precipitation connected to westerly winds towards Norway. The efficiency of this deposition, on the other hand, depends on the degree of oxidation during the transport from the emission areas. Efficient oxidation increases the fraction of HNO_3 relative to NO_2 which subsequently gives an increased deposition rate of nitrogen.

The reason for the difference between 1992 and 1995 is therefore most likely explained by reduced transport from the North Sea emission areas to South Norway in 1995 compared with 1992. In addition it is probable that the photochemical oxidation in the atmosphere was less efficient in 1995 compared to 1992. On average, the summer of 1995 was more cloudy and cold than in 1992, causing a slower and less efficient conversion of NO_x to HNO_3, in line with the model results presented here. As mentioned, emission data for 1992 for the North Sea was used in the calculations for both 1992 and 1995. Thus, the lower calculated contribution from the North Sea in 1995 compared to 1992 is not due to any long-term improving trend.

5.2 Ozone concentrations and exposure

5.2.1 Time series of ozone at background monitoring sites

The results for the ozone calculations are shown as time series for each month for the two monitoring sites Kårvatn and Voss in Figure 16, giving the daily maximum ozone concentration observed and calculated.

It is difficult to evaluate the model calculations based on the comparisons presented in Figure 16. Characteristic spikes in the data are seen in the model results as well as in the observations, but the correlation between model calculations and observations is rather variable.

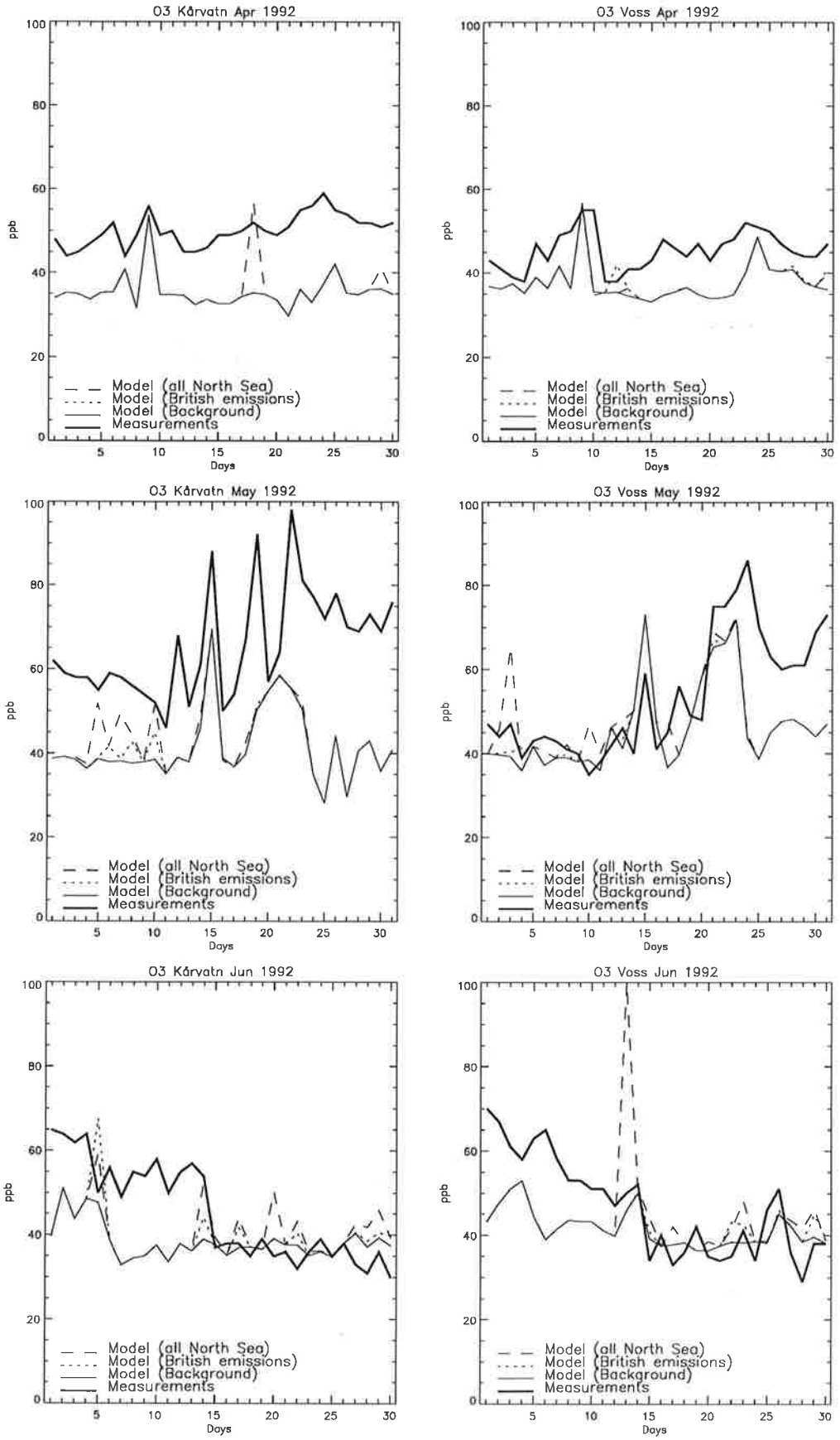

Figure 16: Measured and calculated daily maximum ozone concentration (ppb) at Kårvatn (left) and Voss (right) in May-August 1992.

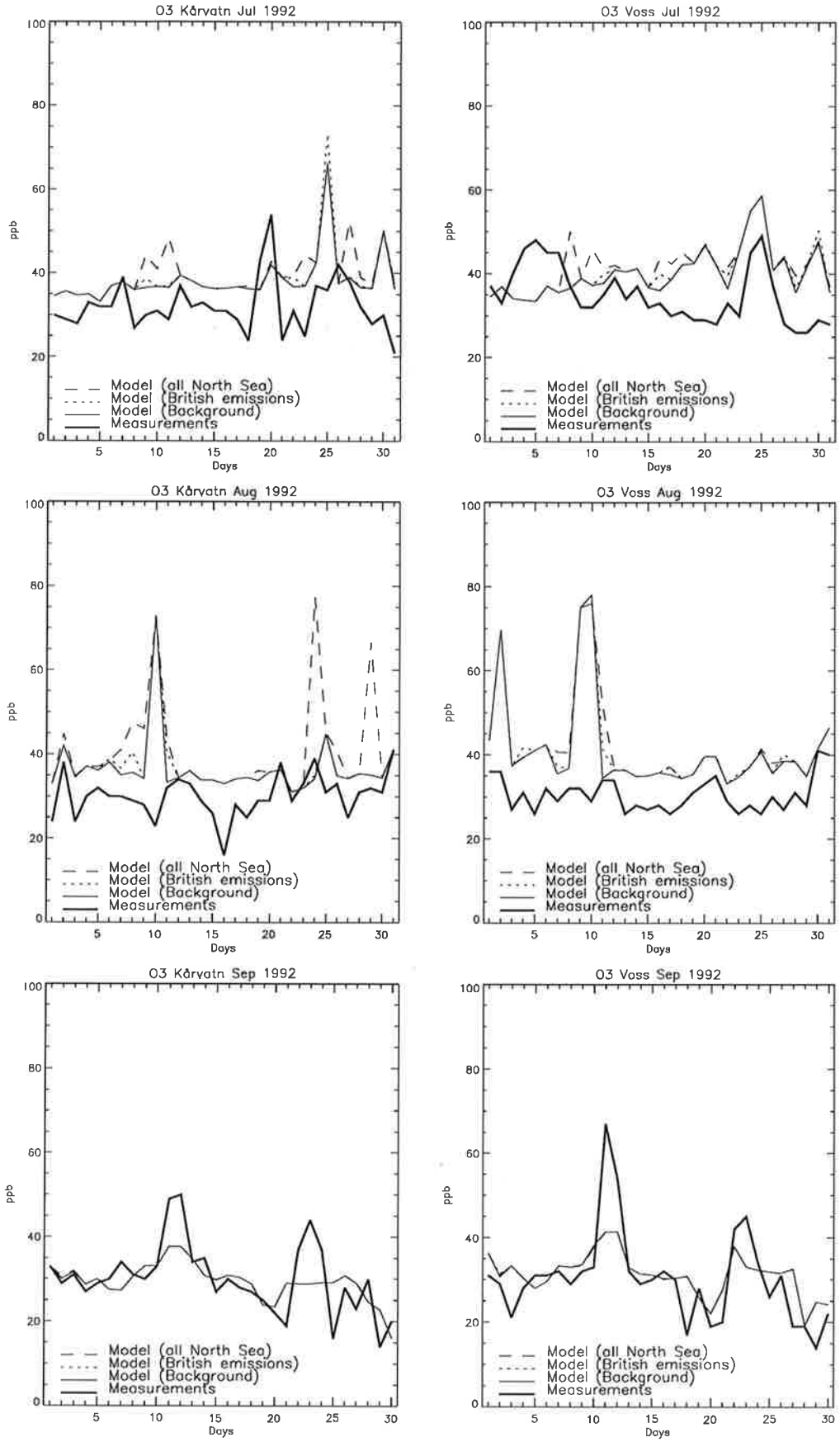

Figure 16, cont.

We want to stress that it is an ambitious task to try to match the calculations of single plumes from the North Sea with observations at 2-3 sites in Southern Norway. The meteorological data have a resolution of 150 km spatially and 6h temporally. The individual plumes from the North Sea will typically have a cross-sectional width of 20-80 km when arriving at the coast of South Norway, i.e. much less than the spatial resolution of the wind fields. The model's wind fields are therefore too coarse to be able to simulate short-term episodes by North Sea emission plumes accurately in time and space at the arrival sites. This does not imply that the model is inadequate, merely that the calculated plumes are displaced somewhat in time and space compared with the actual ones. Thus, when averaged over a sufficiently long time period, the model results are realistic.

This puts certain constraints on the application of the Fotoplume model when used with the present resolution of meteorological data. The model is applicable for studying long-term average quantities, as the AOT40 exposure doses or annual deposition of nitrogen. The model could also be used for estimating frequency distributions, provided that a sufficient time period of simulation is taken together. If the model is to be used for studying specific pollution episodes from the North Sea, and compare that with background measurements, meteorological data with a finer resolution is needed.

However, the time series of ozone shown in Figure 16 gives an impression of how the model behaves compared to representative measurements in the region. In most periods the contribution from the point sources in the North Sea is insignificant. On the other hand, in a few episodes, the model calculates very high concentrations. In fact the calculated model values could even be higher than the one showed, but were not allowed to exceed 100 ppb in the output.

The highest of these peaks are clearly too high when compared with the observations. The explanation for these high spikes in the model results is probably the adding of the individual plumes. In situations with several overlapping plumes it is not surprising that a simple addition of the excess ozone for all plumes gives too high values. It is well known that the ozone formation is non-linear, and, in general, decreases with increased load of emissions.

Figure 17 shows the observed and calculated time series of ozone with 1995 meteorology. The calculations for 1995 indicate that the North Sea emissions contribute to the ozone concentration at Kårvatn and Voss in a few episodes only. The contribution in the first three months, April-June, show particularly low contributions from the North Sea, probably due to weather conditions unfavourable for ozone formation from the west.

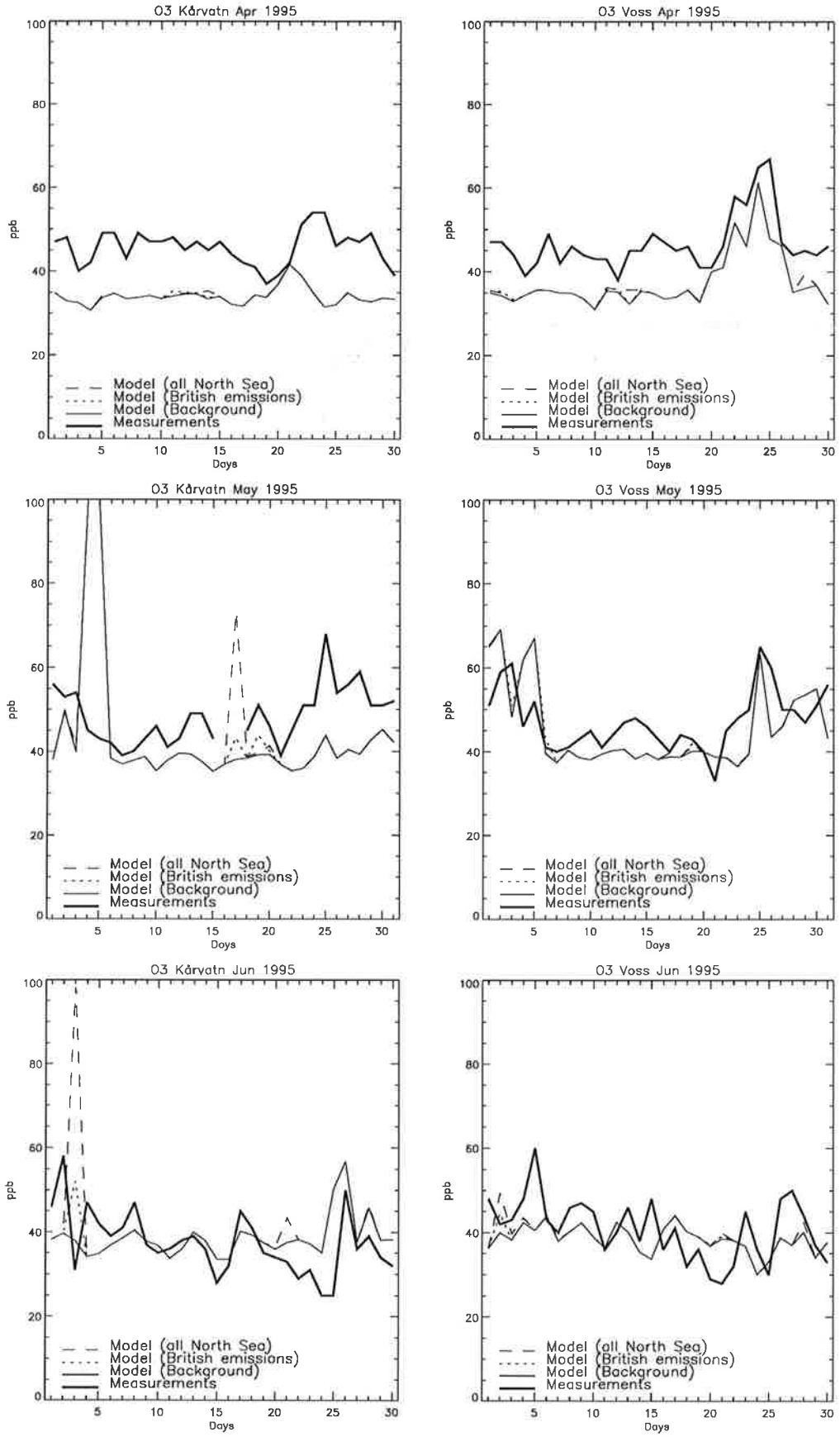

Figure 17: Measured and calculated daily maximum ozone concentration (ppb) at Kårvatn (left) and Voss (right) for May-August 1995.

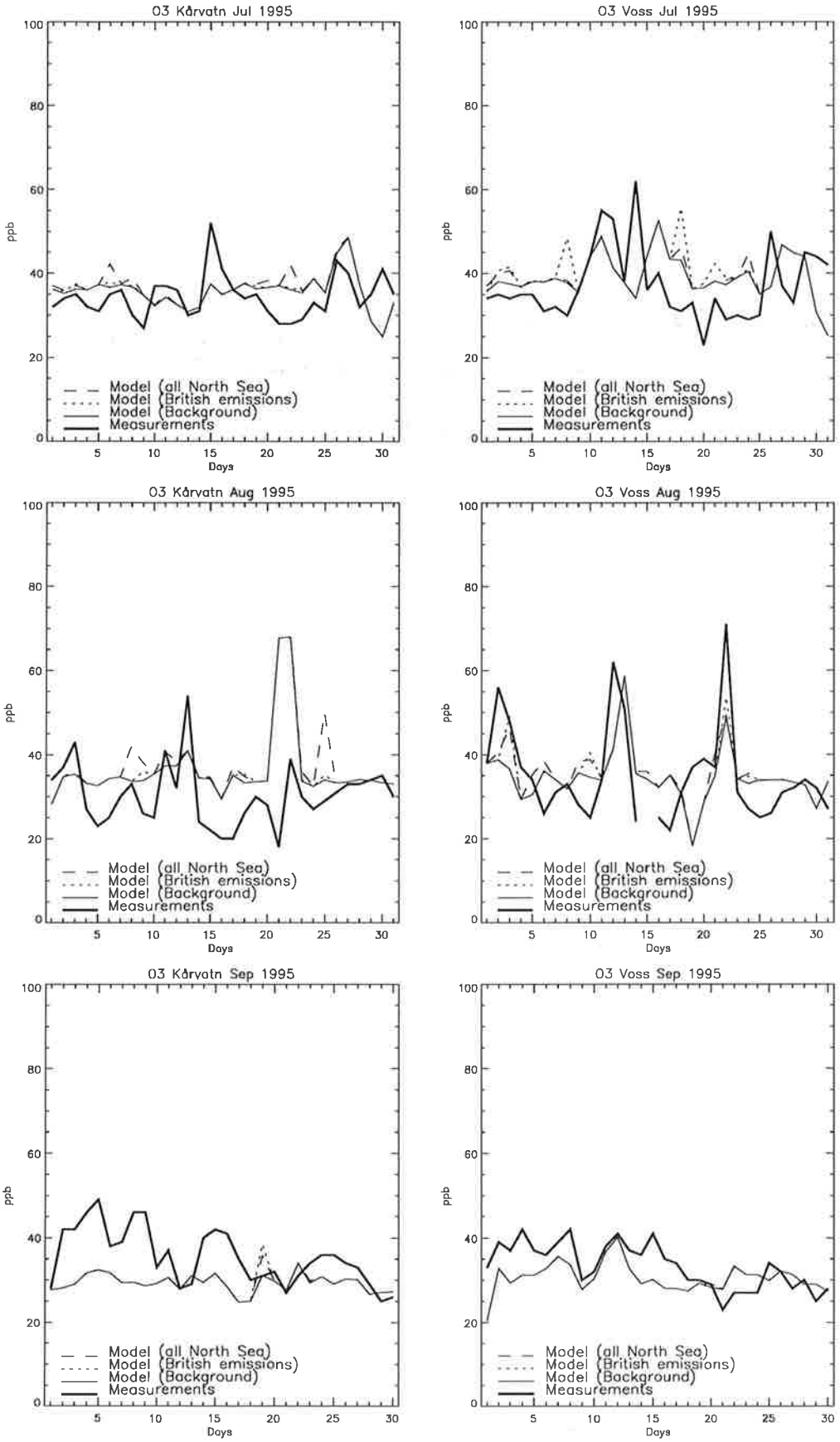

Figure 17, cont.

5.2.2 Estimation of AOT40

AOT40 is defined as the time integrated ozone concentrations above 40 ppb during the growth season, and are normally expressed in the unit ppbhours. The critical level of ozone was previously set to an AOT40 value of 10 000 ppbhours. That corresponds to a 10 per cent growth reduction measured in open chamber-experiments for 6 species through a six-months period (April-September). For crops a critical level of 5 000 ppbhours over a three-months' period has been used.

In the last years there has been some revisions to the critical levels connected to AOT40. As the growth season in Scandinavia obviously is different from that at the European continent, a growth season modified for Nordic countries has been recommended. Table 9 shows the growth season as a function of latitude used in the present calculations. Ozone values for all the day's 24 hours were used in the calculations.

Table 9: The growth season for coniferous trees/meadows as a function of the latitude assumed in the calculation of AOT40.

Latitude (°N)	Growth season
< 62	15 Apr - 30 Sep
62-65	1 May - 30 Sep
65-69	15 May - 15 Sep

The assumed start of the growth season may have a large influence on the estimated AOT40 as the mean ozone concentration in South Norway normally peaks in April-May. The seasonal cycle of the average ozone concentration in Scandinavia is characterized by a sine-like function with a peak in April-May and a minimum in the autumn. Figure 18 shows the average seasonal cycle of ozone for Birkenes and Voss based on all hourly measurements from 1990-1994. Monthly percentiles are also given in the Figure. Even tough the AOT40 index is a long-term integrated quantity, there will be large variations from one year to another. The reason for this is, as indicated by Figure 18, that the threshold of 40 ppb is close to the background level, i.e. the large scale mean, in periods of the year.

Furthermore, it has been recommended to use a 5% growth reduction limit instead of the previous 10% limit. This implies that a critical level of 3000 ppbhours is recommended for plants. The critical level of ozone exposure for trees is highly uncertain. It is therefore common to still use the value of 10 000 ppbhours as a critical level for forests.

Figure 19 shows the interpolated field of AOT40 for coniferous trees (and meadow) for 1992 and 1995 based on observations. As for the observational fields of nitrogen deposition, it is important be aware that the geographical distribution is uncertain. The fields are based on interpolation of ozone observations at a few background monitoring sites. Thus, the geographical

distribution only express the general broad features in Southern Norway. Locally, there may be large deviations from the AOT40 values shown in Figure 19.

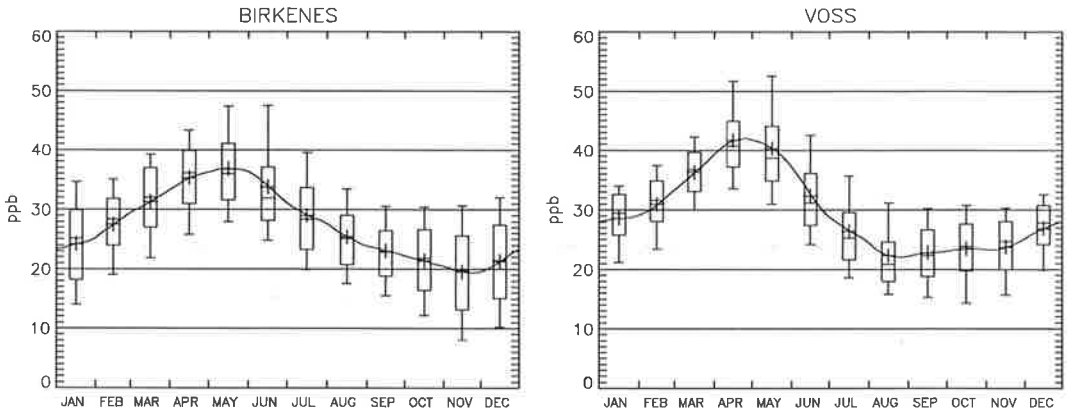

Figure 18: Average seasonal cycle of ozone based on measurements at Birkenes and Voss during 1990-1994. The box and whiskers show the 10-, 25-, 50-, 75- and 90-percentiles.

In 1992 the AOT40 for coniferous/meadows was highest in the south-eastern part of the influence region, peaking at 10,000 – 13,000 ppbhours in Agder. In the rest of the influence region the AOT40 values were in the range 6000 – 9000 ppbhours, except in Nord-Trøndelag which showed values of 1300 – 3000 ppbhours. The AOT40 values in 1995 were lower, peaking at 5000 – 6000 ppbhours in Agder. In the rest of the influence region the values were in the range 1300 – 5000 ppbhours.

The measurements from these two years give an indication of the expected span of AOT40 values from one year to another. Based on comparison with AOT40 values calculated for the ten last years, 1992 was a year with particularly high AOT40 in South Norway, whereas 1995 was on the low side. As discussed above most of the contribution to the AOT40 value is coming from periods in May-June, and very little from August and later. The general ozone level and the number of elevated episodes in May-June are therefore often decisive for that year's AOT40 value. May 1992 was characterized by a higher average ozone level in Southern Scandinavia than normally seen, thus the AOT40 was also high at many sites in South Norway.

Figure 20 shows the calculated absolute and relative contribtution to the AOT40 value in 1992 from Norwegian and British sector, respectively. Figure 21 shows the similar results using 1995-meteorology. The largest contribution from Norwegian sector in 1992 is calculated in Sogn og Fjordane with up to 325 ppbhours near Stad. The calculations indicate contributions from Norwegian sector of 130-200 ppbhours in a zone along the coast from Rogaland to Trøndelag. Else, inland and far south and far north, the contributions from Norwegian sector is calculated to be less than 100 ppbhours in 1992. The contribution from British sector in 1992 is less, peaking at 169 ppbhours in Rogaland, but is mostly less than 100 ppbhours elsewhere in Norway.

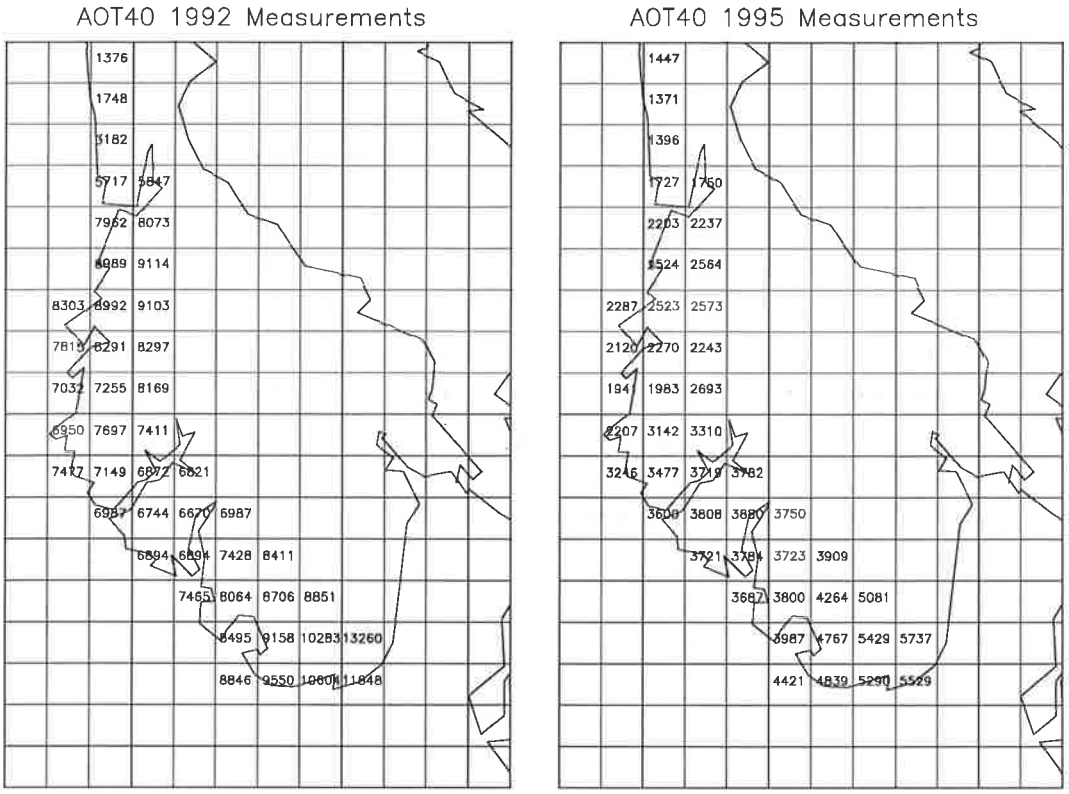

Figure 19: AOT40 values (ppbhours) for coniferous trees and meadows in the receptor points based on measurements at background sites in 1992 (left) and 1995 (right).

The results indicate that emissions from the North Sea from British and Norwegian sector separately contribute to less than 5% each of the AOT40 values for coniferous/meadow.

The calculated influence to the AOT40 value in 1995 is lower (in absolute units) than in 1992. Emissions from Norwegian sector are calculated to contribute with 120-130 ppbhours at most in some coastal areas of Hordaland and Sogn og Fjordane. Else the contribution from Norwegian sector is calculated to be less than 100 ppbhours. The contribution from British sector is also less in 1995 compared with 1992, and is lower than 100 ppbhours in all receptor points. The calculations indicate that Norwegian and British sector separately contributed less than 5% each of the measured AOT40 values in 1995. Relative to the observed AOT40 the calculated percentage contributions from the North Sea were similar using 1992 meteorology and 1995 meteorology. This is because both the observations and the calculated North Sea contributions were lower in 1995 compared to 1992.

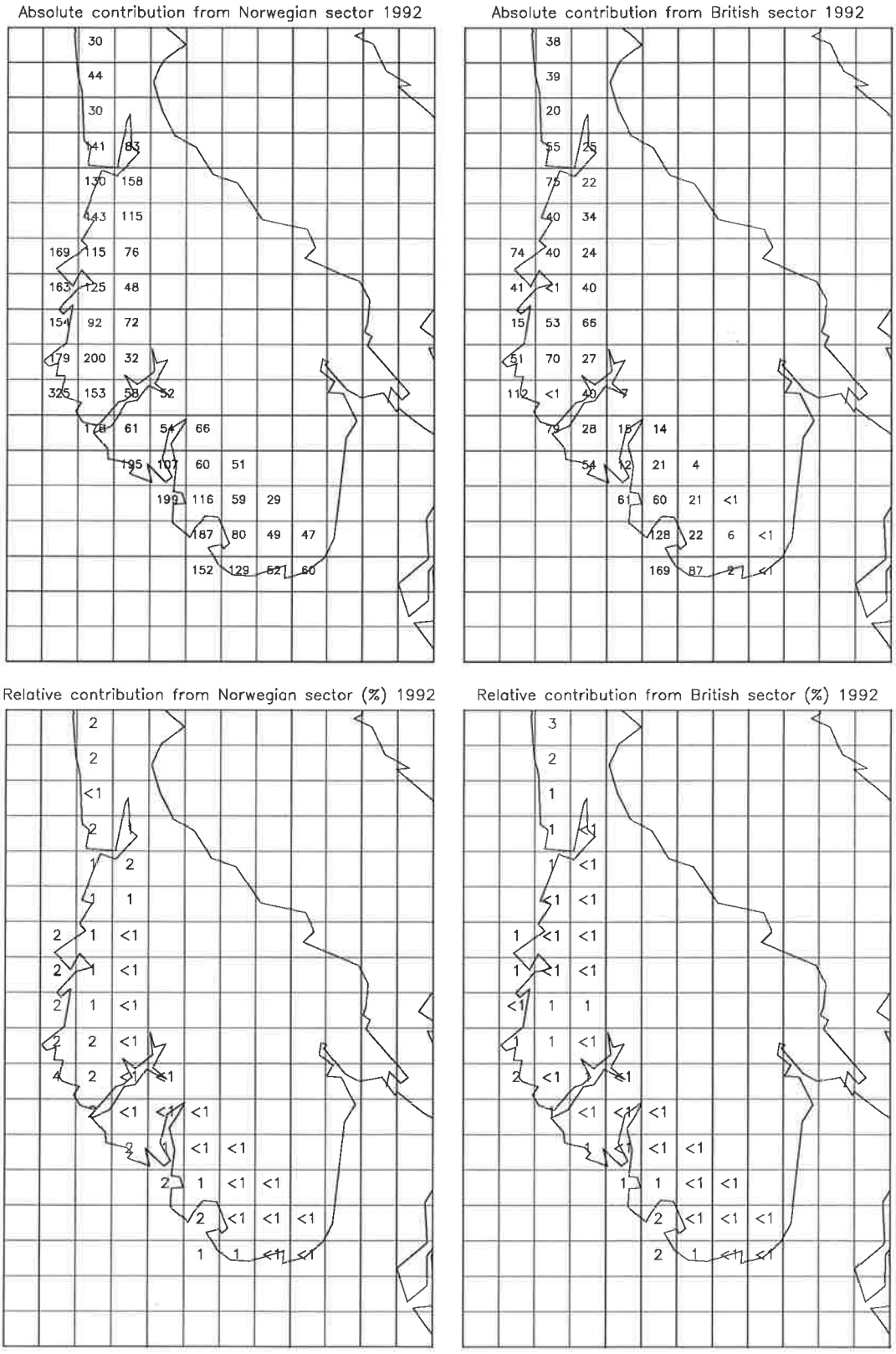

Figure 20: Contribution to the AOT40 values for coniferous trees and meadows in the receptor points in 1992 from emissions in the Norwegian sector (left) and British sector (right). The upper row give the absolute contributions (ppbhours) and the lower row give the relative contributions.

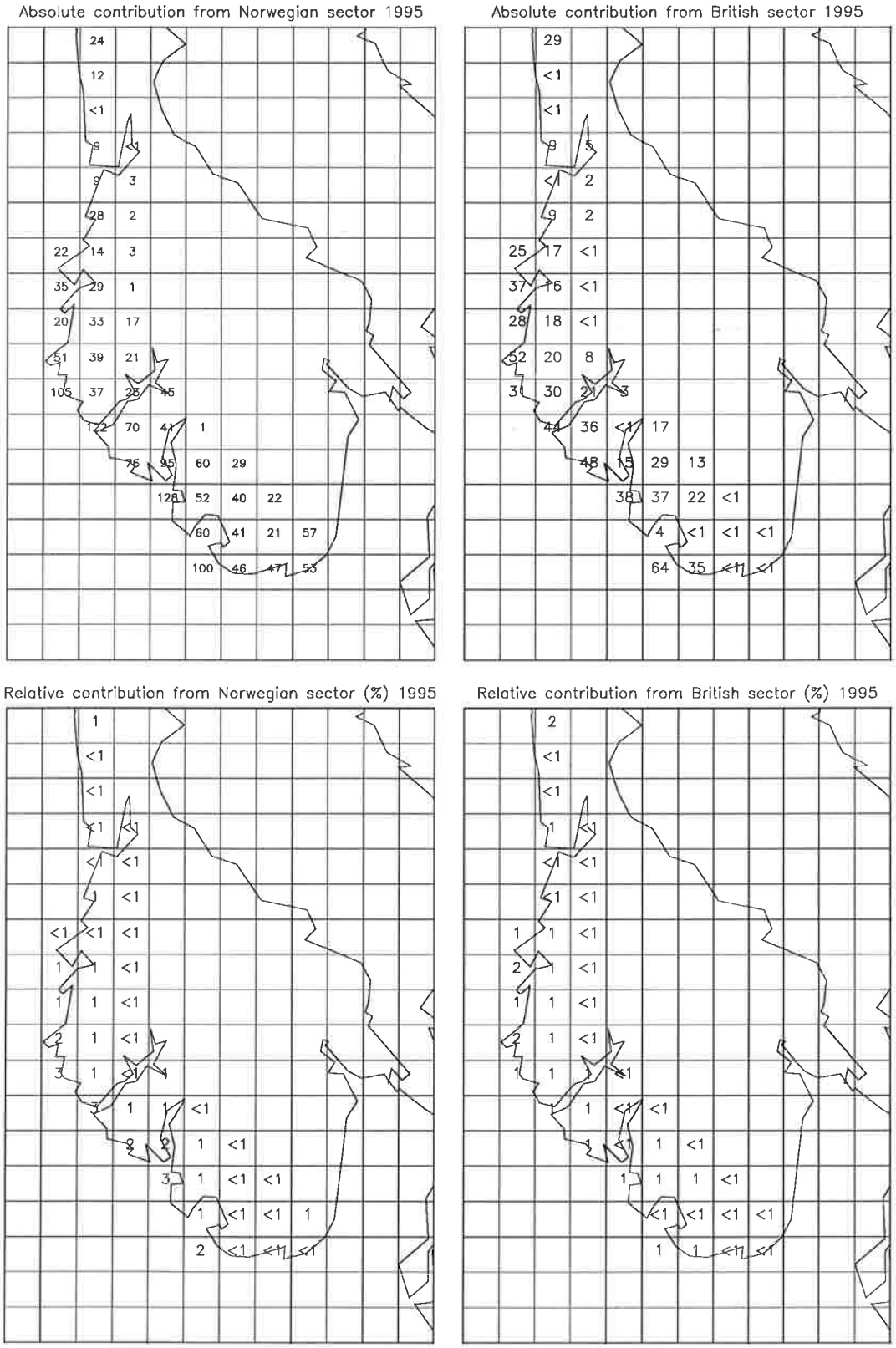

Figure 21: Contribution to the AOT40 values for coniferous trees and meadows in the receptor points in 1992 from emissions in the Norwegian sector (left) and British sector (right). The upper row give the absolute contributions (ppbhours) and the lower row give the relative contributions.

The observations indicate that the critical level for trees was exceeded in Agder (above 10 000 ppbhours) in 1992, but not in 1995. The critical level for meadows, which is indicative of the critical level for plants in general, of 3000 ppbhours was exceeded in most of the influence area in 1992. In 1995 the whole area south of Stad exceeded this limit. Thus, in 1992, all the contribution from emissions in the North Sea came on top of an ozone exposure already exceeding the critical level for meadows. In 1995 the same was true south of Stad. In Sogn og Fjordane the AOT40 level in 1995 was close to the 3000 ppbhours limit, and the contribution from the North Sea emissions may have caused this limit to be exceeded in some areas which would not have experienced exceedance without the North Sea contribution.

5.3 Model evaluation - comparison with previous model results

Table 10 shows the modelled contributions to the N-deposition in 1992 calculated in this report as compared with the values reported by Semb et al. (1996) given in brackets. In general, the new version of Fotoplume gives substantially lower estimates for the North Sea contribution to the nitrogen deposition than the previous calculations. The numbers in Table 10 are, however, not directly comparable. Firstly, deposition processes were not included in the previous version of Fotoplume, instead the N-deposition was inferred from the atmospheric concentrations of NO_2 and HNO_3 and assumed dry deposition velocities. Secondly, the previously estimated relative contributions in Table 10 (adopted from Table 12 in Semb et al. (1996)) referred to the six months' period April-September.

Table 10: Total annual N-deposition (oxidised + reduced) at monitoring sites as deduced from measurements, and the contribution in per cent from Norwegian and British petroleum sector in the North Sea calculated with the new version of Fotoplume. The previous model estimates of the contributions are given in parenthesis.

	Total N-deposition deduced from measurements (mg (N)/m^2)	Estimated contribution from Norwegian sector (%)	Estimated contribution from British sector (%)
Birkenes	1485	<1 (9)	<1 (17)
Skreådalen	1540	<1 (14)	<1 (21)
Voss	810[a]	1 (8)	1 (16)
Kårvatn	303	2 (3)	1 (7)

a) As dry deposition estimates were not available for Voss, the total N-deposition in the 50 km grid square containing Voss was used.

These reservations could, however, not explain the large difference in the new and previous model results. It is quite obvious that the new version of Fotoplume in general calculates much lower contributions to the N-deposition.

Based on this comparison, it is natural to ask the question if the new model version is "better", i.e. gives more realistic results. This was partly studied in the validation report by Solberg et al. (1998), but not for the North Sea situation. One way to evaluate the model is by checking the mass balance of nitrogen. Table 11 compares the total N deposition from Norwegian and British sector with the emissions.

Table 11: Total NO_x emissions from Norwegian and British sector, calculated N deposition in the influence area in South Norway from these two sectors and the resulting fraction of the emitted nitrogen deposited.

	Total NO_X emissions (tonnes (N)/year)	Total N deposition in influence area (tonnes (N)/year)	Relative fraction of NO_X emissions deposited (%)
Norwegian sector	13614	1707	13
British sector	27102	1030	4

For 1992 as a whole 13% of the nitrogen emitted from Norwegian sector is deposited in the influence region, i.e. in the 45 receptor grid cells. Only 4% of the British emissions are deposited in the influence area. It is not possible to perform a similar mass balance calculation for the previous model results. The data in Table 10 (together with the results in Table 11) indicate, however, that the previous estimates would give an unreasonable fraction of the emitted nitrogen deposited in South Norway.

The fraction, f, of the emissions deposited in the influence area may be expressed in a simplistic way as:

$$f = f_{transp} \cdot f_{chem} \cdot f_{dep}$$

where

f_{transp} = the frequency of transport from the emission area to the influence area.
f_{chem} = the fraction of nitrogen "surviving" the transport to the influence area.
f_{dep} = the efficiency of the deposition process in the influence area.

We assume f_{transp} = 40%, i.e. 40% probability of transporting a North Sea plume into the influence area in South Norway

Furthermore, f_{chem} and f_{dep} may be estimated from the expression by Semb et al. (1996), where j equals f_{chem} and $(1-f_{dep})$, respectively:

$$j = e^{-1/h(v_{d,1} \cdot t_1 + v_{d,2} \cdot t_2)} (1-p)$$

f_{chem} is then equal to the so-called correction factor calculated for Stavanger in Table 2 by Semb et al. (1996). This assumes a net deposition rate of 0.5 cm/s over sea, 300 km transport distance from the Norwegian sector to the coast of Norway,

a mean wind speed of 8 m/s, a mixing height of 1000 m, and a precipitation probability of 30%. This gives $f_{chem} = 0.53$.

f_{dep} is estimated in a similar way, assuming a deposition rate of 5 cm/s over land, a cross-sectional distance of 150 km for the influence area, a mean wind speed of 5 m/s, a mixing height of 1000 m and a precipitation probability factor of 50%. This gives $f_{dep} = 89\%$. Taken together these factors give:

$$f = f_{transp} \cdot f_{chem} \cdot f_{dep} = 0.4 \cdot 0.53 \cdot 0.89 = 0.19$$

This simple consideration indicate that for an emission source with 300 km transport distance from the Norwegian coast in the order of 20% of the total emissions will be deposited in a 150 km coastal zone over land.

This estimate is, of course, highly simplified and uncertain. It is, however, indicative of the magnitude of a reasonable deposition rate. Considering that parts of the emissions from the Norwegian sector has a longer transport distance than 300 km from the coast, the simple estimate of 20% corresponds well with the overall 13% calculated by the Fotoplume model.

A similar simplistic approach for the British emissions is even more uncertain due to the larger spread of emission sources. However, assuming 50% longer transport distance, and a probability of 30% for a plume reaching the influence area in South Norway we end up with $f = 0.12$ for British sector. This is still significantly higher than the 4% calculated by Fotoplume. The reason for this discrepancy must be explained by processes in Fotoplume more effective than represented by the simplistic equation above. A possible explanation is that more of the nitrogen is deposited as HNO_3 to the sea surface during the transport towards the Norwegian coast, or, alternatively, that the meteorological situation was even less favourable for transport from the British sector to South Norway.

For the ozone calculations, it is not straightforward to compare the new calculations with the previous results presented by Semb et al (1996), partly because the growth season is different (all six months was used in the previous report). However, it is quite clear that the new calculations also give substantially lower contributions from the North Sea emissions to the AOT40 values than calculated previously. Table 12 gives the absolute contribution from the Norwegian and British sector to the AOT40 index for 1992 for three monitoring sites as calculated now compared with previous values in the report by Semb et al (1996) in brackets.

Differences in the estimated contribution to AOT40 between the new and previous model calculations could have several explanations. Firstly, the different growth seasons in the two model calculations are not taken into account. Secondly, the previous model results were not linked to the observed values, whereas the present procedure is only used to estimate relative differences in AOT40 in two model scenarios (explained in section 4.5), whereas the "standard" calculation is forced to match the observed AOT40. The large changes in estimated AOT40, shown in Table 12, is therefore not reflecting equally large changes in the photochemical processes.

Table 12: Calculated contribution to the AOT40 for coniferous/meadow from Norwegian sector compared with the previous calculations in Semb et al. (1996) in brackets.

	Contribution from the North Sea emissions to AOT40 (ppbh)	
	from Norwegian sector	from British sector
Birkenes	47 (384)	6 (868)
Voss	54 (297)	15 (903)
Kårvatn	115 (140)	34 (430)

6. Conclusions

The effects of atmospheric emissions from oil and gas exploration activity in the North Sea for nitrogen deposition and ozone exposure in Southern Norway have been studied. The emissions include nitrogen oxides (NO_x), carbon monoxide (CO) and volatile organic compounds (VOC). The study reported here is a follow-up after a first project phase.

The calculated total contribution to the N-deposition from the North Sea in 1992 show maxima in the coastal areas of Hordaland and Sogn og Fjordane. The calculations give contributions of 40-50 mg (N)/m^2 and 20-30 mg (N)/m^2 for Norwegian and British sectors, respectively, totalling 60-80 mg (N)/m^2 in this region. The largest *relative* contribution from the North Sea is calculated in Møre og Romsdal. Here the calculations give contributions of 10-13% for each of Norwegian and British sector compared to the total nitrogen deposition in 1992, totalling 20% for the North Sea contribution. The calculations give a marked maximum zone in N-deposition from the North Sea emissions along the coast, whereas the calculated deposition drops inland. Only a minor contribution from the North Sea emissions to the N-deposition is found in the most exposed areas in the southern part (Agder).

The calculated contribution from the North Sea to the nitrogen deposition, using 1995-meteorology instead of 1992 (but with the same 1992 emissions) gives lower deposition values than in 1992. This regards particularly the contribution from Norwegian sector. With 1995-meteorology the maximum area of influence from the Norwegian sector is displaced somewhat to the south. The geographical pattern of N-deposition of North Sea emissions in 1995 is, however, rather similar the one calculated for 1992. As the same emission data (for 1992) were used in both the calculations for 1992 and 1995, the differences in the calculated North Sea contribution is purely due to meteorological differences.

The model was used to estimate the contributions to ozone exposure expressed by the so-called AOT40 index. The results indicate that emissions from British and Norwegian sector separately contribute less than 5% each of the measured AOT40 values for coniferous/meadow. In 1992 the Norwegian sector of the North Sea is calculated to contribute up to 325 ppbhours near Stad. The calculations indicate contributions from Norwegian sector of 130-200 ppbhours in a zone along the coast from Rogaland to Trøndelag, and less than 100 ppbhours else.

The calculated influence to the AOT40 value using 1995-meteorology is lower (in absolute units) than in 1992. The contribution from British sector is also less in 1995 compared with 1992, and is lower than 100 ppbhours in all receptor points. Relative to the observed AOT40 the calculated percentage contributions from the North Sea were similar using 1992 meteorology and 1995 meteorology. This is because both the observations and the calculated North Sea contributions were lower in 1995 compared to 1992.

The new version of Fotoplume calculates much lower contributions both to the N-deposition and to the AOT40 index than previous model versions. With the new version 13% of the nitrogen emitted from Norwegian sector is calculated to deposit in the receptor points for 1992 as a total, slightly less than estimated simplistically. Compared with the previous results in Semb et al. (1996) this shows that the recent model development, and in particular the parameterisation of deposition processes, have given more realistic model results.

The new calculations have also give substantially lower contributions from the North Sea emissions to the AOT40 values than calculated previously. This reflects both a generally improved model and a more sophisticated procedure for estimating the AOT40 index.

7. Acknowledgement

The comments and recommendations during the project from the reference group for OLF, consisting of Karl Henrik Bryne, Laila Iren Helgesen, Ulf Einar Moltu and Henning Natvig Lie, have been of great value for the preparation of this report. We are grateful for the preparation of the measurement data of nitrogen deposition made by Kjetil Tørseth at NILU. We would also like to thank David Simpson (DNMI) for kindly providing the software used in the interpolation of ozone concentrations and AOT40 calculations.

8. References

Andersson-Sköld, Y. and Simpson, D. (1999) Comparison of the chemical schemes of the EMEP MSC-W and IVL photochemical trajectory model. *Atmos. Environ.*, *33*, 1111-1129.

Bøhler, T. (1996) MEPDIM. The NILU Meteorological Processor for Dispersion Modelling. Version 1.0. Model description. Kjeller (NILU TR 7/96).

Dollard, G.J., Atkins, D.H.F., Davies, T.J. and Healy, C. (1987) Concentrations and dry deposition velocities of nitric acid. *Nature*, *326*, 481-483.

Eliassen, A. and Saltbones, S. (1983) Modelling of long-range transport of sulphur over Europe. A two-year model run and some model experiments. *Atmos. Environ.*, *17*, 1457-1473.

EMEP MSC-W (1998) Transboundary Acidifying air pollution in Europe. Estimated dispersion of acidifying and eutrophying compounds and comparison with observations. EMEP MSC-W Status report 1998 – Part 1.

Hass, H., Builtjes, P.J.H., Simpson, D. and Stern, R. (1997) Comparison of model results obtained with several European regional air quality models. *Atmos. Environ., 19*, 3259-3279.

Johansson, C. and Granat, L. (1987) An experimental study of the dry deposition of gaseous nitric acid to snow. *Atmos. Environ., 21*, 1165-1170.

Knudsen, S., Aarrestad, P.A. and Skjelkvåle, B.L. (1996a) Konsekvenser av utslipp til luft fra gasskraftverk Kollsnes. Kjeller (NILU OR 24/96) (in Norwegian).

Knudsen, S., Johnsrud, M., Solberg, S., Walker, S.E. and Skjelkvåle, B.L. (1996b) Utslipp fra petroleumsrelatert aktivitet på Haltenbanken. Bidrag til fotokjemisk oksidantdannelse og forsuring. Kjeller (NILU OR 6/96) (in Norwegian).

Kuhn, M. et al. (1998) Intercomparison of the gas-phase chemistry in several chemistry and transport models. *Atmos. Environ., 4*, 693-709.

Meixner, F.X., Franken, H.H., Duijzer, J.H. and van Aalst, R.M. (1988) Dry deposition of gaseous HNO_3 to a pine forest. In: *Air Pollution modelling and its Application VI*. Ed. by H. van Dop. New York, Plenum. pp. 23-35.

Olsen, H., Polak, K. and Stendal, L. (1993) Måling av avgass fra tankbåt ved lasting på Sture. Norsk Hydro produksjon a.s. (Teknisk rapport nr. 93-33037) (in Norwegian)

Semb, A. and Solberg, S. (1993) Eventuell ozondannelse under lasting av olje ved Sture. Lillestrøm (NILU brevrapport O-1676) (in Norwegian).

Semb, A., Schjoldager, J. and Knudsen, S. (1995) Omvandling og avsetning av nitrogenforbindelser i atmosfæren over hav og kystnære områder. Kjeller (NILU OR 10/95) (in Norwegian).

Semb, A., Knudsen, S., Kraabøl, A. G., Schjoldager, J., Solberg, S. and Walker, S.E. (1996) Effects of the Norwegian oil industry's emissions in the North Sea on ozone exposure levels and nitrogen deposition in Southern Norway. Kjeller (NILU OR 58/95).

Simpson, D. (1992) Modelling the effect of NO_x and VOC emissions from the Troll field on ozone concentrations in Europe. DNMI (delrapport B VOC).

Simpson, D., Guenther, A., Hewitt, C.N., and Steinberger, R. (1995) Biogenic emissions in Europe. Estimates and uncertainties. *J. Geophys. Res., 100*, 22875-22890.

Solberg, S., Dye, C., Schmidbauer, N. and Simpson, D. (1995) Evaluation of the VOC measurement programme within EMEP. Kjeller, Norwegian Institute for Air Research (EMEP/CCC-Report 5/95).

Solberg, S., Semb, A., Walker, S. E. and Knudsen, S. (1998) Validering og forslag til forbedring av modellen Fotoplume. Forstudie. Kjeller (NILU OR 49/98) (in Norwegian).

Solberg, S., Skjelkvåle, B.L., Aarrestad, P.A., Reitan, O. and Walker, S.E. (1999) Regional konsekvensutredning for oljevirksomheten i Nordsjøen. Tema-rapport 5: Regulære utslipp til luft – konsekvenser (in Norwegian).

Tørseth, K., Hansen, A., Simpson, D. and Solberg, S. (1998) Estimates of crop damage in Norway due to exposure to surface ozone, for the year 2010. Statens Forurensningstilsyn (report in preparation).

Appendix A

Emission tables

Table A.1: Name and type of emission sources in the Norwegian sector, as well as the corresponding megasource and the grid coordinates x and y referring to Figure 3. UTM_x and UTM_y is the east and north UTM coordinates, using the WGS84 system and zone 31. The emission numbers give the emitted mass in tonnes/year of NO, NO_2, CH_4, CO and VOC.

Megasource	x	y	Name	Type	UTM_x	UTM_y	NO	NO2	CH4	CO	VOC
1	13	10	2/4 A	Cold vent	513707	6264211	0	0	244	0	157
1	13	10	2/4 A	Diesel engines	513742	6264246	90	7	0	44	10
1	13	10	Flare South	Cold vent	513500	6266650	0	0	0	0	0
1	13	10	Flare South	Flare	513500	6266650	16	1	1	3	0
1	13	10	Safe Lancia	Diesel engines	513335	6266935	71	6	0	34	8
1	13	10	Neddrill Kolskaya	Diesel engines	513435	6267055	24	2	0	11	3
1	13	10	Rigmar	Diesel engines	513285	6267085	50	4	0	24	6
1	13	10	2/4 H	Diesel engines	513135	6267151	4	0	0	2	0
1	13	10	2/4 C	Cold vent	513236	6267209	0	0	244	0	157
1	13	10	2/4 C	Diesel engines	513271	6267244	93	8	0	45	11
1	13	10	2/4 P	Cold vent	513133	6267301	0	0	244	0	157
1	13	10	2/4 P	Fugitive	513133	6267301	0	0	294	0	171
1	13	10	2/4 P	Turbines	513168	6267336	214	17	38	93	10
1	13	10	2/4 T	Cold vent	513065	6267394	0	0	244	0	157
1	13	10	Tananger/ Sola	Helicopter traffic	513065	6267394	46	4	0	323	0
1	13	10	Interfield transport	Helicopter traffic	513065	6267394	13	1	0	88	0
1	13	10	Interfield transport	Stand by ships	513065	6267394	44	4	0	14	5
1	13	10	Tananger/ Sola	Supply ships	513065	6267394	786	63	0	254	91
1	13	10	Interfield transport	Supply ships	513065	6267394	278	22	0	90	32
1	13	10	2/4 T	Turbines	513065	6267394	2070	167	387	902	102
1	13	10	2/4 R	Cold vent	513013	6267517	0	0	244	0	157
1	13	10	2/4 R	Turbines	513048	6267552	153	12	44	67	12
1	13	10	Flare North	Cold vent	512950	6267670	0	0	0	0	0
1	13	10	Flare North	Flare	512950	6267670	128	10	4	21	1
1	13	10	2/4 B&K	Flare	512570	6269186	3	0	0	0	0
1	13	10	2/4 B&K	Cold vent	512650	6269186	0	0	244	0	157
1	13	10	2/4 B&K	Diesel engines	512685	6269221	98	8	0	48	11
1	13	10	2/4 B&K	Turbines	512685	6269221	709	57	86	309	23
2	6	17	SPM-C	Loading buoys	441168	6794760	0	0	1600	0	34067
2	6	17	Statfjord A	Cold vent	438509	6791968	0	0	244	0	157
2	6	17	Statfjord A	Helicopter traffic	438509	6791968	7	1	0	50	0
2	6	17	Statfjord A	Stand by ships	438509	6791968	53	4	0	17	6
2	6	17	Statfjord A	Supply ships	438509	6791968	43	4	0	14	5
2	6	17	Statfjord A	Diesel engines	438484	6791995	136	11	0	66	16
2	6	17	Statfjord A	Turbines	438526	6792008	805	65	126	351	33
2	6	17	Statfjord A	Flare	438509	6792108	245	20	8	40	2
2	6	17	OLS-A	Loading buoys	441332	6792784	0	0	1600	0	34067
2	6	18	Statfjord C	Cold vent	441197	6796479	0	0	81	0	73
2	6	18	Statfjord C	Helicopter traffic	441197	6796479	7	1	0	50	0
2	6	18	Statfjord C	Stand by ships	441197	6796479	53	4	0	17	6
2	6	18	Statfjord C	Supply ships	441197	6796479	43	4	0	14	5
2	6	18	Statfjord C	Turbines	441246	6796523	1091	88	177	475	47
2	6	18	Statfjord C	Flare	441197	6796626	164	13	5	26	1
3	6	17	Gullfaks A	Diesel engines	456416	6782750	9	1	0	4	1
3	6	17	Gullfaks A	Helicopter traffic	456386	6782785	7	1	0	50	0
3	6	17	Gullfaks A	Stand by ships	456386	6782785	26	2	0	9	3
3	6	17	Gullfaks A	Supply ships	456386	6782785	43	4	0	14	5
3	6	17	Gullfaks A	Turbines	456416	6782800	1035	84	170	451	45
3	6	17	Gullfaks A	Cold vent	456386	6782907	0	0	81	0	73
3	6	17	Gullfaks A	Flare	456386	6782907	208	17	7	34	2
3	6	17	SPM-1	Loading buoys	455706	6784583	0	0	3705	0	17275
3	6	17	SPM-2	Loading buoys	459560	6781820	0	0	3705	0	17275

Megasource	x	y	Name	Type	UTM_x	UTM_y	NO	NO2	CH4	CO	VOC
3	6	18	Gullfaks C	Diesel engines	460615	6785412	10	1	0	5	1
3	6	18	Gullfaks C	Helicopter traffic	460585	6785447	7	1	0	50	0
3	6	18	Gullfaks C	Stand by ships	460585	6785447	26	2	0	9	3
3	6	18	Gullfaks C	Supply ships	460585	6785447	43	4	0	14	5
3	6	18	Gullfaks C	Turbines	460615	6785462	615	50	101	268	27
3	6	18	Gullfaks C	Cold vent	460585	6785569	0	0	81	0	73
3	6	18	Gullfaks C	Flare	460585	6785569	305	25	10	49	2
3	6	18	Gullfaks B	Diesel engines	457100	6785807	6	1	0	3	1
3	6	18	Gullfaks B	Helicopter traffic	457078	6785817	7	1	0	50	0
3	6	18	Gullfaks B	Other sources	457078	6785817	0	0	0	0	0
3	6	18	Gullfaks B	Stand by ships	457078	6785817	26	2	0	9	3
3	6	18	Gullfaks B	Supply ships	457078	6785817	43	4	0	14	5
3	6	18	Gullfaks B	Cold vent	457078	6785930	0	0	81	0	73
3	6	18	Gullfaks B	Flare	457078	6785930	89	7	3	14	1
4	8	17	Oseberg A&B	Diesel engines	490481	6706361	37	3	0	18	4
4	8	17	Oseberg A&B	Turbines	490481	6706361	1144	92	168	498	45
4	8	17	Oseberg A&B	Cold vent	490511	6706435	0	0	162	0	146
4	8	17	Oseberg A&B	Flare	490511	6706461	355	29	11	57	3
5	6	17	OLS-B	Loading buoys	438650	6788500	0	0	1600	0	34067
5	6	17	Statfjord B	Cold vent	437165	6786558	0	0	81	0	73
5	6	17	Statfjord B	Helicopter traffic	437165	6786558	7	1	0	50	0
5	6	17	Statfjord B	Stand by ships	437165	6786558	53	4	0	17	6
5	6	17	Statfjord B	Supply ships	437165	6786558	43	4	0	14	5
5	6	17	Statfjord B	Turbines	437214	6786602	882	71	142	384	37
5	6	17	Statfjord B	Flare	437165	6786705	178	14	6	29	1
6	7	17	Veslefrikk	Diesel engines	494514	6738818	258	21	0	125	30
6	7	17	Veslefrikk	Helicopter traffic	494554	6738818	7	1	0	50	0
6	7	17	Veslefrikk	Stand by ships	494554	6738818	79	6	0	26	9
6	7	17	Veslefrikk	Supply ships	494554	6738818	130	11	0	42	15
6	7	17	Veslefrikk	Turbines	494514	6738828	273	22	43	119	12
6	7	17	Veslefrikk	Cold vent	494514	6738858	0	0	81	0	73
6	7	17	Veslefrikk	Flare	494514	6738858	102	8	3	16	1
7	14	9	PCP	Turbines	524561	6237160	430	35	71	187	19
7	14	9	PCP	Cold vent	524561	6237180	0	0	244	0	157
7	14	9	PCP	Stand by ships	524561	6237180	129	10	0	42	15
7	14	9	PCP	Supply ships	524561	6237180	92	7	0	30	11
7	14	9	PCP	Diesel engines	524594	6237180	73	6	0	36	8
7	14	9	PCP	Flare	524491	6237220	54	4	2	9	0
8	6	18	Snorre TLP	Cold vent	454172	6813253	0	0	81	0	73
8	6	18	Snorre TLP	Helicopter traffic	454172	6813253	3	0	0	22	0
8	6	18	Snorre TLP	Stand by ships	454172	6813253	24	2	0	8	3
8	6	18	Snorre TLP	Supply ships	454172	6813253	192	15	0	62	22
8	6	18	Snorre TLP	Flare	454092	6813257	183	15	6	30	1
8	6	18	Snorre TLP	Turbines	454190	6813271	32	3	5	14	1
8	6	18	Snorre TLP	Diesel engines	454217	6813273	325	26	0	158	38
9	16	9	B11	Turbines	598096	6147458	723	58	134	315	35
9	16	9	B11	Cold vent	598131	6147493	0	0	430	0	213
9	16	9	B11	Diesel engines	598131	6147493	4	0	0	2	0
10	19	8	H7	Turbines	696541	6044546	713	58	132	311	35
10	19	8	H7	Cold vent	696576	6044581	0	0	449	0	219
10	19	8	H7	Diesel engines	696576	6044581	3	0	0	1	0
11	8	17	Oseberg C	Diesel engines	487700	6719328	159	13	0	77	18
11	8	17	Oseberg C	Turbines	487700	6719328	322	26	50	140	13
11	8	17	Borgila Dolphin	Diesel engines	487730	6719353	137	11	0	66	16
11	8	17	Oseberg C	Cold vent	487700	6719408	0	0	81	0	73
11	8	17	Oseberg C	Flare	487700	6719428	64	5	2	10	1
12	8	17	Brage	Helicopter traffic	502600	6712000	16	1	0	114	0
12	8	17	Brage	Stand by ships	502600	6712000	149	12	0	48	17
12	8	17	Brage	Supply ships	502600	6712000	390	32	0	126	45
13	8	15	TCP2	Diesel engines	447778	6638390	5	0	0	2	1

Megasource	x	y	Name	Type	UTM_x	UTM_y	NO	NO2	CH4	CO	VOC
13	8	15	TCP2	Turbines	447799	6638396	391	32	73	171	19
13	8	15	TCP2	Other sources	447769	6638415	5	0	13	0	7
13	8	15	TCP2	Cold vent	447804	6638421	0	0	1697	0	212
13	8	15	TP1	Diesel engines	447585	6638405	2	0	0	1	0
13	8	15	TP1	Cold vent	447638	6638408	0	0	970	0	184
13	8	15	QP elf	Diesel engines	447665	6638219	3	0	0	1	0
13	8	15	QP elf	Helicopter traffic	447658	6638231	8	1	0	54	0
13	8	15	QP elf	Other sources	447658	6638231	3	0	0	0	0
13	8	15	QP elf	Stand by ships	447658	6638231	42	3	0	14	5
13	8	15	QP elf	Supply ships	447658	6638231	40	3	0	13	5
13	8	15	DP2	Diesel engines	448090	6639072	5	0	0	2	1
13	8	15	FP	Cold vent	447150	6638609	0	0	530	0	20
14	13	9	2/7 FTP	Flare	516219	6248050	3	0	0	1	0
14	13	9	2/7 FTP	Cold vent	516419	6248050	0	0	244	0	157
14	13	9	2/7 FTP	Diesel engines	516454	6248085	15	1	0	7	2
14	13	9	2/7 FTP	Turbines	516454	6248085	231	19	45	101	12
14	13	9	2/7 B	Flare	513320	6252894	3	0	0	1	0
14	13	9	2/7 B	Cold vent	513470	6252894	0	0	244	0	157
14	13	9	2/7 B	Diesel engines	513505	6252929	60	5	0	29	7
14	13	9	2/7 B	Turbines	513505	6252929	141	11	29	62	8
15	12	10	Ula	Flare	490880	6330507	71	6	2	12	1
15	12	10	Ula	Cold vent	490915	6330525	0	0	81	0	73
15	12	10	Ula	Helicopter traffic	490915	6330525	3	0	0	24	0
15	12	10	Ula	Stand by ships	490915	6330525	28	2	0	9	3
15	12	10	Ula	Supply ships	490915	6330525	66	5	0	21	8
15	12	10	Ula	Diesel engines	490895	6330543	8	1	0	4	1
15	12	10	Ula	Turbines	490935	6330543	249	20	61	109	16
16	7	17	Ross Rig	Diesel engines	463399	6770926	384	31	0	186	44
17	8	15	HMP1	Turbines	456420	6604338	205	17	36	89	10
17	8	15	HMP1	Diesel engines	456424	6604344	4	0	0	2	1
17	8	15	HMP1	Cold vent	456403	6604358	0	0	508	0	116
17	8	15	HMP1	Helicopter traffic	456420	6604364	2	0	0	12	0
17	8	15	HMP1	Stand by ships	456420	6604364	20	2	0	7	2
17	8	15	HMP1	Supply ships	456420	6604364	40	3	0	13	5
17	8	15	HMP1	Flare	456420	6604472	4	0	0	1	0
17	8	15	HMP1	Other sources	456420	6605364	17	1	45	0	25
18	6	18	Transocean No.8	Diesel engines	469076	6799153	287	23	0	139	33
19	8	16	West Alpha	Diesel engines	456177	6668840	284	23	0	138	33
20	13	10	Gyda	Flare	504986	6306399	35	3	1	6	0
20	13	10	Gyda	Cold vent	505076	6306399	0	0	81	0	73
20	13	10	Gyda	Helicopter traffic	505076	6306399	3	0	0	24	0
20	13	10	Gyda	Stand by ships	505076	6306399	28	2	0	9	3
20	13	10	Gyda	Supply ships	505076	6306399	66	5	0	21	8
20	13	10	Gyda	Turbines	505076	6306409	128	10	30	56	8
20	13	10	Gyda	Diesel engines	505056	6306417	5	0	0	3	1
21	14	9	West Delta	Diesel engines	515375	6243204	248	20	0	120	29
22	7	17	Ross Isle	Diesel engines	481301	6746170	231	19	0	112	27
23	11	11	Deepsea Bergen	Diesel engines	458351	6371555	206	17	0	100	24
24	8	18	Vildkat	Diesel engines	545327	6744539	194	16	0	94	22
25	13	10	2/4 D	Cold vent	505258	6268892	0	0	244	0	157
25	13	10	2/4 D	Diesel engines	505293	6268927	181	15	0	88	21
26	13	9	West Vanguard	Diesel engines	494061	6268008	134	11	0	65	15
27	8	15	Odin 30/10	Flare	453501	6660439	4	0	0	1	0
27	8	15	Odin 30/10	Cold vent	453524	6660439	0	0	288	0	163
27	8	15	Odin 30/10	Helicopter traffic	453577	6660439	1	0	0	4	0
27	8	15	Odin 30/10	Stand by ships	453577	6660439	8	1	0	2	1
27	8	15	Odin 30/10	Supply ships	453577	6660439	58	5	0	19	7
27	8	15	Odin 30/10	Diesel engines	453597	6660444	1	0	0	0	0
27	8	15	Odin 30/10	Turbines	453597	6660444	12	1	6	5	1
28	13	10	2/4 E	Flare	519902	6277718	1	0	0	0	0

Megasource	x	y	Name	Type	UTM_x	UTM_y	NO	NO2	CH4	CO	VOC
28	13	10	2/4 E	Cold vent	520052	6277718	0	0	244	0	157
28	13	10	2/4 E	Diesel engines	520087	6277753	27	2	0	13	3
28	13	10	2/4 E	Turbines	520087	6277753	54	4	11	24	3
29	10	12	Blokk 16/11-S	Turbines	468953	6449977	9	1	5	4	1
29	10	12	Blokk 16/11-S	Helicopter traffic	468983	6449977	1	0	0	5	0
29	10	12	Blokk 16/11-S	Stand by ships	468983	6449977	7	1	0	2	1
29	10	12	Blokk 16/11-S	Supply ships	468983	6449977	65	5	0	21	8
29	10	12	Blokk 16/11-S	Cold vent	468958	6449997	0	0	124	0	77
30	13	10	2/4 F	Cold vent	502284	6275259	0	0	244	0	157
30	13	10	2/4 F	Diesel engines	502319	6275294	53	4	0	26	6
31	13	9	2/7 C + Tommeliten	Flare	506286	6257948	5	0	0	1	0
31	13	9	2/7 C + Tommeliten	Cold vent	506436	6257948	0	0	244	0	157
31	13	9	2/7 C + Tommeliten	Diesel engines	506471	6257983	29	2	0	14	3
31	13	9	2/7 C + Tommeliten	Turbines	506471	6257983	15	1	8	7	2
32	13	10	1/6 A	Flare	496120	6277764	1	0	0	0	0
32	13	10	1/6 A	Cold vent	496320	6277764	0	0	244	0	157
32	13	10	1/6 A	Diesel engines	496355	6277799	3	0	0	1	0
32	13	10	1/6 A	Turbines	496355	6277799	20	2	11	9	3
33	12	10	7/11 A	Flare	465556	6325400	2	0	0	0	0
33	12	10	7/11 A	Cold vent	465706	6325400	0	0	244	0	157
33	12	10	7/11 A	Diesel engines	465741	6325435	5	0	0	3	1
33	12	10	7/11 A	Turbines	465741	6325435	11	1	6	5	2
34	16	6	QP amoco	Helicopter traffic	525673	6014747	6	0	0	41	0
35	14	9	Hod	Cold vent	528577	6225945	0	0	81	0	73

Table A.2: Name and type of emission sources in the British sector, as well as the corresponding megasource and the grid coordinates x and y referring to Figure 3. UTM_x and UTM_y is the east and north UTM coordinates, using the WGS84 system and zone 31. The emission numbers give the emitted mass in tonnes/year of NO, NO_2, CH_4, CO and VOC.

Megasource	x	y	Name	type	UTM_x	UTM_y	NO	NO2	CH4	CO	VOC
1	6	17	Brent	Cold vent	432011	6779347	0	0	419	0	226
1	6	17	Brent	Diesel engines	432011	6779347	2068	167	0	1001	238
1	6	17	Brent	Flare	432011	6779347	1655	134	53	267	13
1	6	17	Brent	Turbines	432011	6779347	1231	99	288	537	76
2	9	12	Miller	Cold vent	407589	6512481	0	0	267	0	144
2	9	12	Miller	Diesel engines	407589	6512481	593	48	0	287	68
2	9	12	Miller	Flare	407589	6512481	2198	177	71	355	18
2	9	12	Miller	Turbines	407589	6512481	353	28	83	154	22
3	9	10	Forties	Diesel engines	372400	6401102	1342	108	0	650	155
3	9	10	Forties	Flare	372400	6401102	977	79	32	158	8
3	9	10	Forties	Turbines	372400	6401102	799	65	187	348	49
4	8	14	Beryl	Cold vent	416596	6609712	0	0	91	0	49
4	8	14	Beryl	Diesel engines	416596	6609712	936	76	0	453	108
4	8	14	Ness	Diesel engines	416596	6609712	56	5	0	27	6
4	8	14	Beryl	Flare	416596	6609712	1113	90	36	180	9
4	8	14	Ness	Flare	416596	6609712	54	4	2	9	0
4	8	14	Beryl	Turbines	416596	6609712	558	45	131	243	34
4	8	14	Ness	Turbines	416596	6609712	33	3	8	14	2
5	5	18	Magnus	Cold vent	410499	6833288	0	0	419	0	226
5	5	18	Magnus	Diesel engines	410499	6833288	1344	108	0	651	155
5	5	18	Magnus	Flare	410499	6833288	407	33	13	66	3
5	5	18	Magnus	Turbines	410499	6833288	800	65	187	349	49
6	6	16	Ninlan	Cold vent	416939	6748317	0	0	419	0	226
6	6	16	Ninian	Diesel engines	416939	6748317	740	60	0	358	85
6	6	16	Staffa	Diesel engines	416939	6748317	47	4	0	23	5
6	6	16	Ninian	Flare	416939	6748317	597	48	19	96	5
6	6	16	Staffa	Flare	416939	6748317	678	55	22	109	5
6	6	16	Ninian	Turbines	416939	6748317	441	36	103	192	27
6	6	16	Staffa	Turbines	416939	6748317	28	2	7	12	2
7	10	10	Arbroath	Diesel engines	402801	6360904	297	24	0	144	34
7	10	10	Arbroath	Flare	402801	6360904	1927	155	62	311	16
7	10	10	Arbroath	Turbines	402801	6360904	177	14	41	77	11
8	6	17	Alwyn N	Cold vent	431475	6742901	0	0	1269	0	683
8	6	17	Alwyn N	Diesel engines	431475	6742901	1091	88	0	528	126
8	6	17	Alwyn N	Flare	431475	6742901	190	15	6	31	2
8	6	17	Alwyn N	Turbines	431475	6742901	650	52	152	283	40
9	17	5	Morecombe South	Cold vent	544183	5980734	0	0	3004	0	1618
9	17	5	Morecombe South	Diesel engines	544183	5980734	1062	86	0	514	122
9	17	5	Morecombe South	Turbines	544183	5980734	632	51	148	276	39
10	12	9	Fulmar	Cold vent	448162	6262728	0	0	85	0	46
10	12	9	Fulmar	Diesel engines	448162	6262728	738	60	0	357	85
10	12	9	Fulmar	Flare	448162	6262728	380	31	12	61	3
10	12	9	Fulmar	Turbines	448162	6262728	439	35	103	191	27
11	16	2	Leman	Cold vent	442519	5885841	0	0	2609	0	1405
11	16	2	Leman	Diesel engines	442519	5885841	922	74	0	447	106
11	16	2	Leman	Turbines	442519	5885841	549	44	129	239	34
11	16	2	Leven	Diesel engines	442538	5885871	26	2	0	13	3
11	16	2	Leven	Flare	442538	5885871	2	0	0	0	0
11	16	2	Leven	Turbines	442538	5885871	16	1	4	7	1
12	8	11	Piper	Cold vent	340540	6483973	0	0	39	0	21
12	8	11	Piper	Diesel engines	340540	6483973	14	1	0	7	2
12	8	11	Piper	Turbines	340540	6483973	8	1	2	4	1
12	8	11	Claymore	Diesel engines	339924	6483193	409	33	0	198	47
12	8	11	Scapa	Diesel engines	339924	6483193	249	20	0	121	29
12	8	11	Claymore	Flare	339924	6483193	163	13	5	26	1

Megasource	x	y	Name	type	UTM_x	UTM_y	NO	NO2	CH4	CO	VOC
12	8	11	Scapa	Flare	339924	6483193	244	20	8	39	2
12	8	11	Claymore	Turbines	339924	6483193	244	20	57	106	15
12	8	11	Scapa	Turbines	339924	6483193	149	12	35	65	9
13	5	17	Tern	Diesel engines	388709	6799769	636	51	0	308	73
13	5	17	Tern	Flare	388709	6799769	434	35	14	70	4
13	5	17	Tern	Turbines	388709	6799769	379	31	89	165	23
14	8	13	Brae N	Cold vent	405041	6518762	0	0	91	0	49
14	8	13	Brae N	Diesel engines	405041	6518762	357	29	0	173	41
14	8	13	Brae N	Flare	405041	6518762	706	57	23	114	6
14	8	13	Brae N	Turbines	405041	6518762	212	17	50	93	13
15	8	11	Petronella	Diesel engines	329757	6470274	94	8	0	45	11
15	8	11	Petronella	Flare	329757	6470274	136	11	4	22	1
15	8	11	Petronella	Turbines	329757	6470274	56	4	13	24	3
15	8	11	Rob Roy	Cold vent	331638	6471215	0	0	53	0	28
15	8	11	Hamish	Diesel engines	331638	6471215	19	2	0	9	2
15	8	11	Rob Roy	Diesel engines	331638	6471215	328	26	0	159	38
15	8	11	Rob Roy	Flare	331638	6471215	434	35	14	70	4
15	8	11	Hamish	Turbines	331638	6471215	11	1	3	5	1
15	8	11	Rob Roy	Turbines	331638	6471215	195	16	46	85	12
16	9	11	Balmoral	Diesel engines	391253	6456740	239	19	0	116	28
16	9	11	Glamis	Diesel engines	391253	6456740	30	2	0	14	3
16	9	11	Balmoral	Flare	391253	6456740	434	35	14	70	4
16	9	11	Glamis	Flare	391253	6456740	244	20	8	39	2
16	9	11	Balmoral	Turbines	391253	6456740	142	11	33	62	9
16	9	11	Glamis	Turbines	391253	6456740	18	1	4	8	1
17	5	17	Cormorant S	Cold vent	396344	6776006	0	0	419	0	226
17	5	17	Cormorant S	Diesel engines	396344	6776006	335	27	0	162	39
17	5	17	Cormorant S	Flare	396344	6776006	570	46	18	92	5
17	5	17	Cormorant S	Turbines	396344	6776006	199	16	47	87	12
18	10	12	Maureen	Diesel engines	423528	6445126	216	17	0	105	25
18	10	12	Moira	Diesel engines	423528	6445126	17	1	0	8	2
18	10	12	Maureen	Flare	423528	6445126	651	53	21	105	5
18	10	12	Moira	Flare	423528	6445126	27	2	1	4	0
18	10	12	Maureen	Turbines	423528	6445126	129	10	30	56	8
18	10	12	Moira	Turbines	423528	6445126	10	1	2	4	1
19	6	17	Dunlin	Diesel engines	425339	6794802	239	19	0	116	28
19	6	17	Osprey	Diesel engines	425339	6794802	245	20	0	119	28
19	6	17	Dunlin	Flare	425339	6794802	109	9	4	18	1
19	6	17	Osprey	Flare	425339	6794802	54	4	2	9	0
19	6	17	Dunlin	Turbines	425339	6794802	142	11	33	62	9
19	6	17	Osprey	Turbines	425339	6794802	146	12	34	64	9
20	6	18	Thistle	Cold vent	425722	6806494	0	0	419	0	226
20	6	18	Don	Diesel engines	425722	6806494	44	4	0	21	5
20	6	18	Thistle	Diesel engines	425722	6806494	318	26	0	154	37
20	6	18	Don	Flare	425722	6806494	163	13	5	26	1
20	6	18	Thistle	Flare	425722	6806494	163	13	5	26	1
20	6	18	Don	Turbines	425722	6806494	26	2	6	11	2
20	6	18	Thistle	Turbines	425722	6806494	190	15	44	83	12
21	17	3	Indefatigable	Cold vent	468805	5916717	0	0	1595	0	859
21	17	3	Indefatigable	Diesel engines	468805	5916717	564	45	0	273	65
21	17	3	Indefatigable	Turbines	468805	5916717	336	27	79	146	21
22	5	17	Cormorant N	Cold vent	401274	6791498	0	0	419	0	226
22	5	17	Cormorant N	Diesel engines	401274	6791498	398	32	0	193	46
22	5	17	Cormorant N	Flare	401274	6791498	217	18	7	35	2
22	5	17	Cormorant N	Turbines	401274	6791498	237	19	56	103	15
23	6	18	Murchison (UK)	Cold vent	433023	6808636	0	0	419	0	226
23	6	18	Murchison (UK)	Diesel engines	433023	6808636	385	31	0	187	44
23	6	18	Murchison (UK)	Flare	433023	6808636	190	15	6	31	2
23	6	18	Murchison (UK)	Turbines	433023	6808636	229	19	54	100	14
24	5	17	Eider	Diesel engines	402413	6804499	279	23	0	135	32
24	5	17	Eider	Flare	402413	6804499	353	28	11	57	3
24	5	17	Eider	Turbines	402413	6804499	166	13	39	72	10
25	14	3	Ravenspurn North	Cold vent	364211	5994167	0	0	1218	0	656
25	14	3	Ravenspurn North	Diesel engines	364211	5994167	431	35	0	208	50

Megasource	x	y	Name	type	UTM_x	UTM_y	NO	NO2	CH4	CO	VOC
25	14	3	Ravenspurn North	Turbines	364211	5994167	256	21	60	112	16
26	9	10	Kittiwake	Cold vent	353253	6372875	0	0	85	0	46
26	9	10	Kittiwake	Diesel engines	353253	6372875	260	21	0	126	30
26	9	10	Kittiwake	Flare	353253	6372875	244	20	8	39	2
26	9	10	Kittiwake	Turbines	353253	6372875	155	13	36	68	10
27	9	12	Brae S	Cold vent	401021	6507847	0	0	91	0	49
27	9	12	Brae S	Diesel engines	401021	6507847	132	11	0	64	15
27	9	12	Brae S	Flare	401021	6507847	434	35	14	70	4
27	9	12	Brae S	Turbines	401021	6507847	79	6	18	34	5
28	6	17	Hutton NW	Cold vent	409205	6776301	0	0	419	0	226
28	6	17	Hutton NW	Diesel engines	409205	6776301	230	19	0	112	27
28	6	17	Hutton NW	Flare	409205	6776301	244	20	8	39	2
28	6	17	Hutton NW	Turbines	409205	6776301	137	11	32	60	8
29	16	2	Hewett & Della	Cold vent	418089	5884929	0	0	1084	0	584
29	16	2	Hewett & Della	Diesel engines	418089	5884929	383	31	0	186	44
29	16	2	Hewett & Della	Turbines	418089	5884929	228	18	53	99	14
30	6	16	Emerald	Diesel engines	393284	6728113	66	5	0	32	8
30	6	16	Emerald	Flare	393284	6728113	461	37	15	74	4
30	6	16	Emerald	Turbines	393284	6728113	39	3	9	17	2
31	8	11	Ivanhoe	Cold vent	330827	6454157	0	0	53	0	29
31	8	11	Ivanhoe	Diesel engines	330827	6454157	242	20	0	117	28
31	8	11	Ivanhoe	Flare	330827	6454157	136	11	4	22	1
31	8	11	Ivanhoe	Turbines	330827	6454157	144	12	34	63	9
32	12	9	Clyde	Cold vent	456360	6256885	0	0	85	0	46
32	12	9	Clyde	Diesel engines	456360	6256885	248	20	0	120	29
32	12	9	Clyde	Flare	456360	6256885	109	9	4	18	1
32	12	9	Clyde	Turbines	456360	6256885	148	12	35	64	9
33	16	3	Audrey	Cold vent	432049	5936171	0	0	832	0	448
33	16	3	Audrey	Diesel engines	432049	5936171	294	24	0	142	34
33	16	3	Audrey	Turbines	432049	5936171	175	14	41	76	11
34	14	2	Amethyst	Cold vent	354206	5944368	0	0	705	0	380
34	14	2	Amethyst	Diesel engines	354206	5944368	249	20	0	121	29
34	14	2	Amethyst	Turbines	354206	5944368	148	12	35	65	9
35	6	17	Hutton	Diesel engines	413825	6771666	197	16	0	96	23
35	6	17	Hutton	Flare	413825	6771666	81	7	3	13	1
35	6	17	Hutton	Turbines	413825	6771666	118	9	28	51	7
36	8	11	Highlander	Diesel engines	331827	6477153	95	8	0	46	11
36	8	11	Highlander	Flare	331827	6477153	12	1	0	2	0
36	8	11	Highlander	Turbines	331827	6477153	56	5	13	25	3
36	8	11	Tartan	Cold vent	329129	6473801	0	0	40	0	21
36	8	11	Tartan	Diesel engines	329129	6473801	92	7	0	45	11
36	8	11	Tartan	Flare	329129	6473801	81	7	3	13	1
36	8	11	Tartan	Turbines	329129	6473801	55	4	13	24	3
37	8	10	Buchan	Diesel engines	326028	6423924	116	9	0	56	13
37	8	10	Buchan	Flare	326028	6423924	190	15	6	31	2
37	8	10	Buchan	Turbines	326028	6423924	69	6	16	30	4
38	8	10	Angus	Diesel engines	327082	6448156	208	17	0	100	24
38	8	10	Angus	Turbines	327082	6448156	124	10	29	54	8
39	14	3	West Sole	Cold vent	374093	5958018	0	0	577	0	311
39	14	3	West Sole	Diesel engines	374093	5958018	204	16	0	99	24
39	14	3	West Sole	Turbines	374093	5958018	121	10	28	53	7
40	14	3	Ravenspurn South	Cold vent	358107	5994969	0	0	534	0	287
40	14	3	Ravenspurn South	Diesel engines	358107	5994969	189	15	0	91	22
40	14	3	Ravenspurn South	Turbines	358107	5994969	112	9	26	49	7
41	16	3	Viking	Cold vent	456363	5923521	0	0	524	0	282
41	16	3	Viking	Diesel engines	456363	5923521	185	15	0	90	21
41	16	3	Viking	Turbines	456363	5923521	110	9	26	48	7
42	16	3	Vulcan	Cold vent	431632	5902055	0	0	497	0	268
42	16	3	Vulcan	Diesel engines	431632	5902055	176	14	0	85	20
42	16	3	Vulcan	Turbines	431632	5902055	105	8	25	46	6
43	9	13	Brae C	Cold vent	415456	6527988	0	0	91	0	49
43	9	13	Brae C	Diesel engines	415456	6527988	169	14	0	82	20
43	9	13	Brae C	Turbines	415456	6527988	101	8	24	44	6
44	15	3	Clipper	Cold vent	410178	5936537	0	0	472	0	254

Megasource	x	y	Name	type	UTM_x	UTM_y	NO	NO2	CH4	CO	VOC
44	15	3	Clipper	Diesel engines	410178	5936537	167	13	0	81	19
44	15	3	Clipper	Turbines	410178	5936537	99	8	23	43	6
45	16	3	Victor	Cold vent	458253	5909844	0	0	428	0	231
45	16	3	Victor	Diesel engines	458253	5909844	151	12	0	73	17
45	16	3	Victor	Turbines	458253	5909844	90	7	21	39	6
46	11	12	Beatrice	Diesel engines	501309	6442565	129	10	0	62	15
46	11	12	Beatrice	Flare	501309	6442565	27	2	1	4	0
46	11	12	Beatrice	Turbines	501309	6442565	77	6	18	33	5
47	17	3	Welland NW	Cold vent	482471	5870819	0	0	236	0	127
47	17	3	Welland NW	Diesel engines	482471	5870819	83	7	0	40	10
47	17	3	Welland NW	Turbines	482471	5870819	50	4	12	22	3
47	17	3	Welland S	Cold vent	482490	5870850	0	0	166	0	89
47	17	3	Welland S	Diesel engines	482490	5870850	59	5	0	28	7
47	17	3	Welland S	Turbines	482490	5870850	35	3	8	15	2
48	9	12	Deveron	Diesel engines	383020	6471829	10	1	0	5	1
48	9	12	Donan	Diesel engines	383020	6471829	50	4	0	24	6
48	9	12	Deveron	Flare	383020	6471829	11	1	0	2	0
48	9	12	Donan	Flare	383020	6471829	109	9	4	18	1
48	9	12	Deveron	Turbines	383020	6471829	6	1	1	3	0
48	9	12	Donan	Turbines	383020	6471829	30	2	7	13	2
49	5	16	Heather	Diesel engines	388683	6759645	80	6	0	39	9
49	5	16	Heather	Flare	388683	6759645	81	7	3	13	1
49	5	16	Heather	Turbines	388683	6759645	48	4	11	21	3
50	15	3	Barque	Cold vent	402995	5942491	0	0	342	0	184
50	15	3	Barque	Diesel engines	402995	5942491	121	10	0	59	14
50	15	3	Barque	Turbines	402995	5942491	72	6	17	31	4
51	12	9	Auk	Diesel engines	442551	6249968	63	5	0	30	7
51	12	9	Auk	Flare	442551	6249968	81	7	3	13	1
51	12	9	Auk	Turbines	442551	6249968	37	3	9	16	2
52	10	9	Gannet B	Cold vent	379122	6339877	0	0	29	0	15
52	10	9	Gannet C	Cold vent	379122	6339877	0	0	29	0	15
52	10	9	Gannet D	Cold vent	379122	6339877	0	0	29	0	15
52	10	9	Gannet B	Diesel engines	379122	6339877	11	1	0	5	1
52	10	9	Gannet C	Diesel engines	379122	6339877	11	1	0	5	1
52	10	9	Gannet D	Diesel engines	379122	6339877	14	1	0	7	2
52	10	9	Gannet B	Flare	379122	6339877	38	3	1	6	0
52	10	9	Gannet C	Flare	379122	6339877	38	3	1	6	0
52	10	9	Gannet D	Flare	379122	6339877	38	3	1	6	0
52	10	9	Gannet B	Turbines	379122	6339877	6	1	2	3	0
52	10	9	Gannet C	Turbines	379122	6339877	7	1	2	3	0
52	10	9	Gannet D	Turbines	379122	6339877	8	1	2	4	1
53	17	2	Camelot C&S	Cold vent	449042	5869821	0	0	294	0	158
53	17	2	Camelot C&S	Diesel engines	449042	5869821	104	8	0	50	12
53	17	2	Camelot C&S	Turbines	449042	5869821	62	5	15	27	4
54	14	3	Cleeton	Cold vent	351700	5989695	0	0	284	0	153
54	14	3	Cleeton	Diesel engines	351700	5989695	100	8	0	49	12
54	14	3	Cleeton	Turbines	351700	5989695	60	5	14	26	4
55	16	3	Tristan	Cold vent	440307	5908151	0	0	23	0	13
55	16	3	Tristan	Diesel engines	440307	5908151	8	1	0	4	1
55	16	3	Tristan	Turbines	440307	5908151	5	0	1	2	0
55	16	3	Vallant South	Cold vent	440326	5908181	0	0	260	0	140
55	16	3	Vallant South	Diesel engines	440326	5908181	92	7	0	45	11
55	16	3	Vallant South	Turbines	440326	5908181	55	4	13	24	3
56	14	5	Esmond	Cold vent	399132	6050536	0	0	239	0	129
56	14	5	Esmond	Diesel engines	399132	6050536	85	7	0	41	10
56	14	5	Esmond	Turbines	399132	6050536	50	4	12	22	3
56	14	5	Forbes	Cold vent	399151	6050566	0	0	18	0	10
56	14	5	Forbes	Diesel engines	399151	6050566	6	1	0	3	1
56	14	5	Forbes	Turbines	399151	6050566	4	0	1	2	0
57	10	10	Montrose	Diesel engines	403438	6368746	22	2	0	10	2
57	10	10	Montrose	Flare	403438	6368746	109	9	4	18	1
57	10	10	Montrose	Turbines	403438	6368746	13	1	3	6	1
58	17	3	Bure	Cold vent	470269	5881849	0	0	45	0	24
58	17	3	Thames & Wensum	Cold vent	470269	5881849	0	0	155	0	84

Megasource	x	y	Name	type	UTM_x	UTM_y	NO	NO2	CH4	CO	VOC
58	17	3	Bure	Diesel engines	470269	5881849	16	1	0	8	2
58	17	3	Thames & Wensum	Diesel engines	470269	5881849	55	4	0	27	6
58	17	3	Bure	Turbines	470269	5881849	9	1	2	4	1
58	17	3	Thames & Wensum	Turbines	470269	5881849	33	3	8	14	2
58	17	3	Yare	Cold vent	471452	5877361	0	0	41	0	22
58	17	3	Yare	Diesel engines	471452	5877361	14	1	0	7	2
58	17	3	Yare	Turbines	471452	5877361	9	1	2	4	1
59	16	2	Anglia	Cold vent	410511	5914212	0	0	233	0	125
59	16	2	Anglia	Diesel engines	410511	5914212	82	7	0	40	9
59	16	2	Anglia	Turbines	410511	5914212	49	4	11	21	3
60	16	3	Valiant North	Cold vent	436410	5912930	0	0	195	0	105
60	16	3	Valiant North	Diesel engines	436410	5912930	69	6	0	33	8
60	16	3	Valiant North	Turbines	436410	5912930	41	3	10	18	3
61	13	9	Argyll	Diesel engines	487051	6226597	33	3	0	16	4
61	13	9	Argyll	Flare	487051	6226597	27	2	1	4	0
61	13	9	Argyll	Turbines	487051	6226597	20	2	5	9	1
61	13	9	Duncan	Diesel engines	482897	6226859	6	1	0	3	1
61	13	9	Duncan	Flare	482897	6226859	5	0	0	1	0
61	13	9	Duncan	Turbines	482897	6226859	4	0	1	2	0
62	15	2	PickerIII	Cold vent	378539	5932855	0	0	151	0	81
62	15	2	PickerIII	Diesel engines	378539	5932855	53	4	0	26	6
62	15	2	PickerIII	Turbines	378539	5932855	32	3	7	14	2
63	14	5	Gordon	Cold vent	431804	6039695	0	0	138	0	74
63	14	5	Gordon	Diesel engines	431804	6039695	49	4	0	24	6
63	14	5	Gordon	Turbines	431804	6039695	29	2	7	13	2
64	17	3	North & South Sean	Cold vent	488804	5907418	0	0	133	0	72
64	17	3	North & South Sean	Diesel engines	488804	5907418	47	4	0	23	5
64	17	3	North & South Sean	Turbines	488804	5907418	28	2	7	12	2
65	16	3	Vanguard	Cold vent	443652	5915558	0	0	105	0	57
65	16	3	Vanguard	Diesel engines	443652	5915558	37	3	0	18	4
65	16	3	Vanguard	Turbines	443652	5915558	22	2	5	10	1
66	9	11	Cyrus	Diesel engines	409793	6444734	12	1	0	6	1
66	9	11	Cyrus	Flare	409793	6444734	27	2	1	4	0
66	9	11	Cyrus	Turbines	409793	6444734	7	1	2	3	0
67	17	2	Camelot N	Cold vent	443403	5867720	0	0	46	0	25
67	17	2	Camelot N	Diesel engines	443403	5867720	16	1	0	8	2
67	17	2	Camelot N	Turbines	443403	5867720	10	1	2	4	1
68	17	4	Markham	Cold vent	499122	5964515	0	0	24	0	13
68	17	4	Markham	Diesel engines	499122	5964515	9	1	0	4	1
68	17	4	Markham	Turbines	499122	5964515	5	0	1	2	0

Norwegian Institute for Air Research (NILU)
P.O. Box 100, N-2007 Kjeller – Norway

REPORT SERIES	REPORT NO. OR 5/99	ISBN 82-425-1053-9	
SCIENTIFIC REPORT		ISSN 0807-7207	
DATE 7 May 1999	SIGN. Hrystein Hon	NO. OF PAGES 71	PRICE NOK 120,-

TITLE

The contribution to nitrogen deposition and ozone formation in South Norway from atmospheric emissions related to the petroleum activity in the North Sea

PROJECT LEADER

Sverre Solberg

NILU PROJECT NO.

O-97074

AUTHOR(S)

S. Solberg, S.-E. Walker, S. Knudsen, M. Lazaridis, H. J. Beine and A. Semb

CLASSIFICATION *

A

CONTRACT REF.

Karl Henrik Bryne

REPORT PREPARED FOR:
The Norwegian Oil Industry Association
P.O. Box 547
N-4003 STAVANGER
NORWAY

ABSTRACT

A photochemical plume model has been developed and refined. The model is designed to simulate the advection and photochemistry for several simultaneous point sources as well as the atmospheric mixing. The model has been used to calculate nitrogen deposition and ozone formation due to offshore emissions in the North Sea. Based on meteorological data for 1992 the calculations give a total contribution of 60-80 mg (N)/m^2 at most in South Norway. Emissions from British and Norwegian sector is calculated to contribute less than 5% each to the AOT40 index for ozone.

NORWEGIAN TITLE

Bidraget til nitrogenavsetning og ozondannelse i Sør-Norge fra luftutslipp knyttet til petroleumsvirksomheten i Nordsjøen

KEYWORDS		
Nitrogen deposition	Ozone formation	Petroleum activity

ABSTRACT (in Norwegian)

En fotokjemisk plume-modell har blitt utviklet og forbedret. Modellen er laget for å beregne adveksjon og fotokjemi for flere samtidige punktkilder i tillegg til atmosfæriske blandingsprosesser. Modellen har blitt brukt til å beregne nitrogenavsetning og ozondannelse fra offshore-utslipp i Nordsjøen. Basert på meteorologiske data for 1992 gir beregningene et maksimalbidrag på 60-80 mg (N)/m^2 i Sør-Norge. Utslipp fra britisk og norsk sokkel er beregnet å bidra med mindre enn 5% hver til AOT40-indeksen for ozon.

** Classification*

- *A Unclassified (can be ordered from NILU)*
- *B Restricted distribution*
- *C Classified (not to be distributed)*